Slowing The Clearance of An Engineered Kallikrein Inhibitor

Slowing The Clearance of An Engineered Kallikrein Inhibitor

By Ghofran Al-Adimi, B.Sc.

400141708

A Thesis Submitted to the School of Graduate Studies

in Partial Fulfillment of the Requirements for the Degree

Master of Science

Medical Sciences Level II

McMaster University

MASTER OF SCIENCE (2023) McMaster University

(Medical Sciences) Hamilton, Ontario

TITLE: Slowing The Clearance of An Engineered Kallikrein Inhibitor

AUTHOR: Ghofran Al-Adimi B.Sc.

SUPERVISOR: Dr. William P. Sheffield

COMMITTEE MEMBERS: Dr. Geoff Werstuck and Dr. Anthony Chan

NUMBER OF PAGES: xv, 90

Lay Abstract

Hereditary angioedema is a rare genetic condition that results in swelling of the face, hands, feet, abdomen, or throat. The most feared symptom is the swelling of the throat, as it could cause suffocation and death. This rare disease is caused by a deficiency in a protein called C1 inhibitor, which controls processes in the body and prevents inflammation. Therefore, the lack or dysfunction of this protein results in the under-regulation of a cellular pathway, which leads to fluid leakage. One of the drugs available to manage and alleviate attacks is Ecallantide, which functions as a "swelling fighter." It combats inflammation by blocking a pathway that is uncontrolled due to the absence of C1 inhibitor. Although this medication has proven to be effective, it is rapidly eliminated from the bloodstream due to its small size. The purpose of this project was to prolong the circulation of Ecallantide in mice. To achieve our objective, modified Ecallantide was engineered and its behavior in the test tube and in mice was investigated.

Abstract

Plasma kallikrein (PK) is a coagulation factor that activates Factor XII in the contact pathway and generates vasoactive bradykinin from kininogen. C1-esterase inhibitor (C1INH) regulates PK levels. C1INH deficiency manifests as potentially life-threatening hereditary angioedema (HAE). Several drugs are licensed for HAE treatment and/or prophylaxis, including C1INH concentrates and recombinant Ecallantide (rEcall). rEcall is a small protein comprised of the first Kunitz domain of Tissue Factor Pathway Inhibitor and was substituted at seven residues making it a PK-specific inhibitor. rEcall is licensed for HAE treatment, but its short half-life prevents prophylactic application. This project focused on comparing the inhibition of PK and the in vivo clearance of hexahistidine-tagged rEcall (H_6-rEcall) and H_6-rEcall genetically fused to human serum albumin (H_6-rEcall-HSA), or an albumin binding domain (H_6-rEcall-ABD). To determine if the orientation of the constructs contributed to activity and half-life, proteins were reoriented, and HSA was moved from the C- to N-terminus.

Proteins produced were H_6-rEcall (64 amino acids), H_6-rEcall-ABD (110 amino acids), H_6-rEcall-HSA (666 amino acids), H_6-rEcall-HSA, rEcall-H_6 (64 amino acids), and HSA-rEcall-H_6 (666 amino acids). All proteins were expressed in *Pichia pastoris*, secreted, and purified from conditioned media via nickel-chelate chromatography. PK activity was assessed via amidolysis of S2302, and the inhibitory constant (K_i) was determined. Purified proteins were radiolabeled with ^{125}I and injected intravenously into CD1 mice. Acid-precipitable radioactivity in timed blood samples was expressed as a percentage of the peak post-injection value. Values were means ± SD, n = 6.

Next, the role of Lipoprotein related receptor protein 1 (LRPI) or neonatal Fc receptor (FcRn) in rEcall proteins' clearance was examined by performing a competition experiment. In

this experiment, rEcall associated with albumin was co-administered with a competitor ligand that blocked FcRn or LRP1. To further investigate the role of these receptors and the organs responsible for rEcall proteins' clearance, organ distribution was conducted by cannulating mice via the right jugular vein and delivering ^{125}I-rEcall or ^{125}I-HSA-rEcall. The organs analyzed were the kidneys, liver, spleen, and heart.

In vitro, rEcall and its modified proteins had a K_i of ~ 2 – 3 nM. In vivo, fusion proteins behaved similarly and presented some pharmacokinetic enhancements. Two hours post-injection, 50 ± 10% of H_6-rEcall-HSA and 36 ± 6 % of HSA-rEcall-H_6 remained in the circulation vs. 6 ± 2 % of H_6-rEcall and 7 ± 1% of H_6-rEcall-ABD ($p < 0.0001$), while 75 ± 5% of HSA-H_6 was recovered in the circulation.

In the competition experiment, the presence of GST-RAP elevated the recovery of ^{125}I-H_6-rEcall-HSA 2.2-fold, from 37 ± 3 % for GST + H_6-rEcall-HSA to 81 ± 3 % for GST-RAP + H_6-rEcall-HSA. Competition with IVIg also significantly increased the recovery of ^{125}I- H_6-rEcall-HSA, but to a lesser degree, by 1.13-fold (to 42 ± 5% for IVIg + H_6-rEcall-HSA). Similar significant changes were also observed 30 mins after injection, of 2.9- and 1.9-fold, respectively.

Finally, results indicate that albumin changed rEcall's organ distribution. Of the four organs extracted 30 minutes after injection, rEcall-H_6 was predominantly found in the kidneys, and fusion to albumin largely redirected rEcall to the liver. 3.6-fold more HSA-rEcall-H_6 was found in the liver in comparison to rEcall ($p<0.0001$). In contrast, 3.3-fold more rEcall was observed in the kidneys vs. rEcall-HSA ($p<0.0001$).

In conclusion, fusing HSA to either the N- or C-terminus of rEcall extended its plasma residency time and did not impact its function towards PK.

Acknowledgements

I would like to express my deepest gratitude and appreciation to all those who have supported and contributed to the completion of this thesis. First and foremost, I am profoundly grateful to my thesis advisor Dr. William P Sheffield for his guidance, and unwavering support throughout this research journey. His irreplaceable expertise, insights, patience, and encouragement have been instrumental in shaping my experience and progress. I am also grateful to my thesis committee members, Dr. Anthony Chan and Dr. Geoff Werstuck, for their time and constructive feedback. Their valuable input and recommendations have massively supplemented my thesis.

I am forever indebted to Varsha Bhatka, Louise Smith, and Tatiana Barbosa. Varsha taught me everything I now know about in vitro experiments and troubleshooting. She largely assisted me in understanding my project and performing and completing various experiments. Like Varsha, Louise helped me carry out my in vivo experiments. Even on Louise's last day at the laboratory as a research assistant, she still chose to help me with my clearance experiments that required the use of radioactive material. Louise's selflessness and generosity are traits I will always remember and cherish. Following Louise's retirement, I had one more in vivo experiment to complete and Tatiana kindly stepped in. I truly believe that without these three individuals, I would not have achieved as much as I did within the past two years.

Furthermore, I am grateful for our breakroom as it fueled my stomach and social battery by getting to know Negin Tehrani and Antje Ask, who were always kind and supportive. I also extend my heartfelt appreciation to Sangavi Sivanthanan, Tyler Seto, and Mostafa Hamada who have supported me along this obstacle-filled yet rewarding experience. Their words of encouragement, discussions, and exchange of ideas were a constant source of motivation and

inspiration. I am happy to say that I came out of this academic pursuit with a degree and three solid friendships.

Additionally, I would also like to express my gratitude to my family for their unconditional love, reinforcement, and faith in my abilities. Their unswerving support and consideration have powered my resilience through the highs and lows of this academic pursuit. Specifically, my mother (Mona Al-Rei) and grandparents (Abdullah Al-Rei and Rawhaya Aslan), who are more excited for me to graduate than myself. Similarly, my brothers (Zobair and Mohammed) and dearest friends (Sheza, Faheema, Laela, Omars, and Aya) kept me motivated and optimistic when obtaining unforeseen data.

Finally, I am honoured to have attended McMaster University and grateful for the staff of the Medical Sciences Program and Faculty of Pathology and Molecular Medicine, who delivered an enriched academic environment and provided access to resources, libraries, research studies, and laboratories. Their commitment to problem-based learning has assisted in my growth as a researcher.

TABLE OF CONTENTS

LIST OF FIGURES

LIST OF TABLES

LIST OF SYMBOLS AND ABBREVIATIONS

°C	Degrees Celsius
3’	3’ primer region variant
5’	5’ primer region variant
α2M	α2-Macroglobulin
ABD	Albumin Binding Domain
ACEI	Angiotensin-converting enzyme inhibitors
ANOVA	Analysis of variance
AOX1	Alcohol Oxidase 1
AUC	Area Under the Curve
BK	Bradykinin
bp	base pair
BSA	Bovine serum albumin
C1INH	C1 esterase inhibitor
CBS	Canadian Blood Services
C-terminal	Carboxyl-terminal
CR	cysteine-rich complement-type repeats
DNA	Deoxyribonucleic acid
dsDNA	double-stranded DNA
E. coli	Escherichia coli
ECL	Enhanced luminol-based chemiluminescent
ELISA	Enzyme-linked immunosorbent assay
ER	Endoplasmic Reticulum
ESI	Electrospray ionization
F	Factor
FcRn	Neonatal Fc Receptor
FIIa	Thrombin
FVa	activated Factor FV
FVIIa	activated Factor FVII
FVIIIa	activated Factor FVIII
FIXa	activated Factor IX
FXa	activated Factor X
FXIa	activated Factor XI
FXIIa	activated Factor FXII
FXIIIa	activated Factor XIII
$(G4S)_3$	15-codon glycine– serine repeat
gBlock	Gene block
GPI	Glycosylphosphatidylinositol
GST	Glutathione sulfotransferase
H_6-tag	Hexahistidine tag
HAE	Hereditary angioedema
HPLC	High-performance liquid chromatography
hTRIAL	human tumour necrosis factor-related apoptosis-inducing ligand
HSA	Human Serum Albumin
HMWK	High Molecular Weight Kininogen

hLF	Human lactoferrin
IgG	Immunoglobulin G
IVIg	Intravenous immunoglobulin G
K_i	second-order rate constant
K_D	equilibrium dissociation constant
kDa	kilodaltons
KD	Kunitz Domain
KPI-HSA	Kunitz Protease Inhibitor-HSA
Kg	kilogram
LMWK	Low Molecular Weight Kininogen
LRP1	Lipoprotein receptor related protein 1
M	molar
Mean V	average reaction velocity
mg	milligram
min	minutes
mL	milliliter
mM	millimolar
MOBIX	Molecular Biology and Biotechnology Institute, McMaster University
mRNA	messenger ribonucleic acid
MS	Mass spectrometry
MSA	Mouse serum albumin
n	nano
NaCl	sodium chloride
$NaHCO_3$	sodium bicarbonate
NEG	negative control
ng	nanograms
nm	nanometer
nM	nanomolar
Ni-NTA	Nickel-Nitriloacetic acid
N-terminal	amino-terminal
OD	Optical density
Oligos	Oligonucleotides
p	pico
PAGE	polyacrylamide gel electrophoresis
PBS	phosphate buffer saline
PCR	polymerase chain reaction
pd	plasma derived
PEG	polyethylene glycol
PK	Plasma kallikrein
PLSN	Plasmin
pM	picomolar
PreK	Prekallikrein
PS	Protein S
RE	Restriction Enzyme
RAP	Receptor-associated protein
rEcall	Recombinant Ecallantide

SD	standard deviation
SDS	sodium dodecyl sulphate
serpin	serine protease inhibitors
$t_{1/2}$	Half-life
TBST	tris-buffered saline and tween
TF	tissue factor
TFPI	tissue factor pathway inhibitor
μL	microliter
μM	Micromolar
vWF	von Willebrand Factor

Declaration of Academic Achievement

All work presented in this thesis paper was accomplished independently by me, except for the protein radiolabelling and jugular vein cannulation by Louise Smith and Tatiana Barbosa, respectively. Louise was also responsible for tail vein injection in mice.

All requirements prior to the defence of this Master's thesis have been met. I have completed two graduate-level courses, presented my data to my committee annually, and hosted a seminar alongside Dr. Sheffield. In the Fall of 2022, I was a teaching assistant for LIFE SCI 3N03, Nutritional Toxicology. In the winter term of 2023, I was a teaching assistant for HTH SCI 1H06, Human Anatomy and Physiology for Nursing.

1.0 Introduction

1.1 Hemostasis

1.1.1 Primary Hemostasis

Hemostasis is a complex physiological mechanism that stops bleeding events caused by vascular damage. Hemostasis is subdivided into primary and secondary hemostasis. Primary hemostasis works to form a platelet plug to seal the injury site in the vasculature. This process is composed of four main steps: vascular constriction, platelet adhesion, platelet activation, and platelet aggregation. To understand this mechanism, it is important to know that platelets are anucleated small cells that contain dense and alpha granules. These granules carry and release material that contributes to hemostasis (Dorgalaleh et al., 2018).

Upon vessel injury, primary hemostasis is initiated by vascular constriction. The smooth muscle surrounding the endothelium contracts, reducing blood flow to the damaged site. Vessel constriction limits blood loss and exposes the subendothelium, collagen, and von Willebrand factor (vWF). Collagen and vWF are critical for platelet adhesion as they capture and begin platelet plug assembly (Broos et al., 2011). Platelet adhesion occurs when the endothelium releases vWF, which then binds to collagen to form a link between the injured vessel site and platelets. Platelet binding to the damaged vessel wall results in shape change and platelet activation. Subsequently, platelet activation stimulates granule secretion to further facilitate platelet activation, aggregation, and plug formation. Thereafter, secondary hemostasis follows to reinforce and heal the damaged vascular site (McMichael, 2005).

1.1.2 Secondary Hemostasis

Secondary hemostasis is a mechanism that follows and supports primary hemostasis. It incorporates the formation and stabilization of a blood clot. This pathway is known as the coagulation cascade, which includes the activation of various serine and coagulation proteases. Coagulation proteases are produced as inactive zymogens whose activation to functional form are facilitated by proteolytic cleavage. As shown in Figure 1, this cascade is divided into two pathways: the intrinsic and the extrinsic pathway. The two pathways are triggered differently (Dahlbäck, 2000). The extrinsic pathway is initiated when tissue factor (TF), a protein in surrounding tissues, is exposed due to vascular injury. TF forms a complex with Factor VII (FVII) and produces activated Factor VII (FVIIa). The FVIIa then interacts with calcium ions and activates Factor X (FX) (Palta et al., 2014).

In contrast, the intrinsic pathway is stimulated when FXII comes into contact with negatively charged surfaces at the site of injury. This interaction activates Factor XII (FXII), which consequently activates Factor XI (FXI). Activated FXI then proteolytically cleaves Factor IX (FIX). Then, activated FIX, along with non-enzymatic cofactor FVIIIa, phospholipids, and calcium ions, make the intrinsic tenase complex and cleave Factor X (FX) (Norris, 2003).

As in Figure 1, FX activation marks the connection between the intrinsic and extrinsic pathways, also known as the common pathway. The common pathway starts with the formation of the prothrombinase complex, which consists of FXa, FVa, calcium ions, and phospholipids. The prothrombinase complex cleaves Factor II (prothrombin) into FIIa (thrombin). Thrombin plays a major role in coagulation amplification as it further activates serine proteases, activates platelets via Protease-Activated Receptors, and cleaves fibrinogen to insoluble fibrin. Thrombin also activates transglutaminase Factor XIII, which then crosslinks fibrin polymers, creating a mesh-like structure stabilizing the blood clot and platelet plug (Palta et al., 2014).

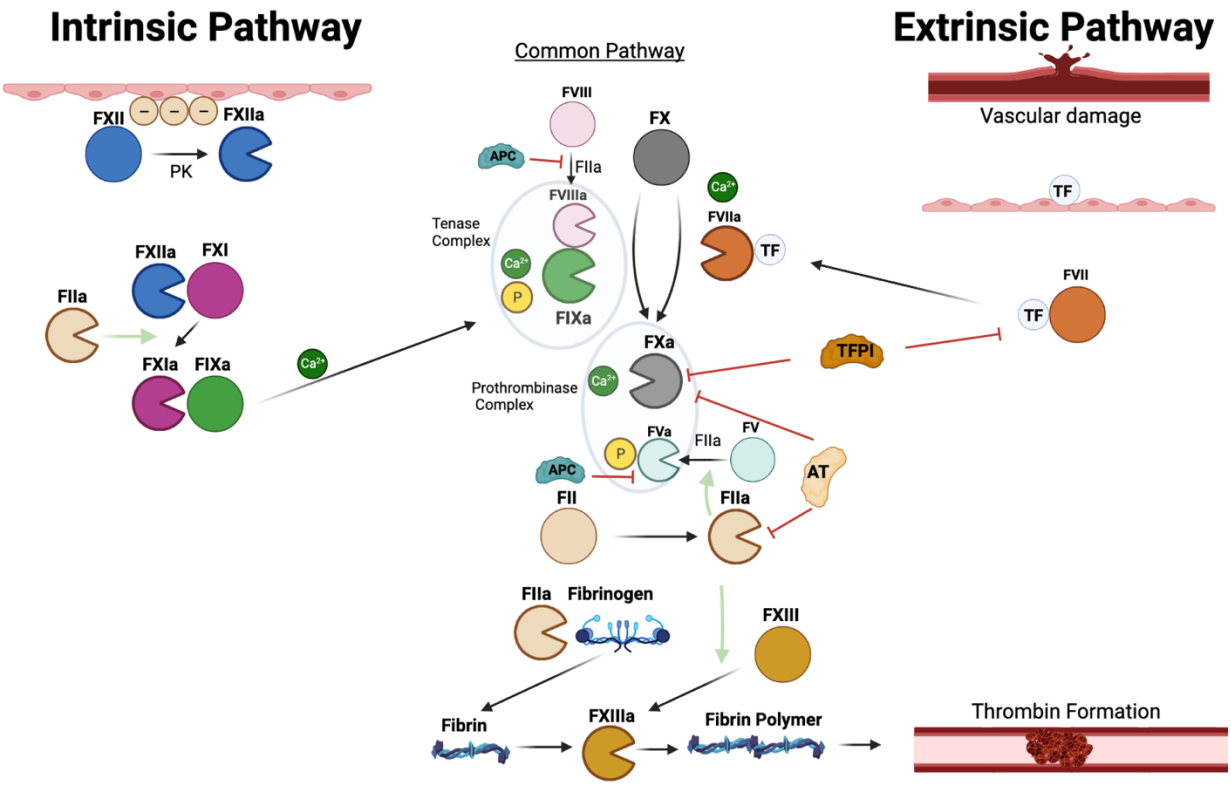

Figure 1: **Secondary hemostasis.** Black, red, and green arrows indicate cleavage, inhibition, and positive feedback, respectively. “Pacemen” represent the activation of proteases via proteolytic cleavage. FXIII, Factor XIII; FXIIIa, activated Factor XIII; FXII, Factor XII; FXIIa, activated Factor XII; FXI, Factor XI; FXIa, activated Factor XI; FX, Factor X; FXa, activated Factor X; FIX, Factor IX; FIXa, activated Factor IX; FVIII, Factor VIII; FVIIIa, activated Factor VIII; FVII, Factor VII; FVIIa, activated Factor VII; FV, Factor V; FVa, activated Factor V; FII, Prothrombin; FIIa, Thrombin; Ca^{2+}, Calcium ions; P, Phospholipids; PK, Plasma Kallikrein; “-” Negatively charged surfaces; TF, Tissue factor; AT, Antithrombin; TFPI, tissue factor pathway inhibitor; APC, activated Protein C.

1.1.2.1 Tissue Factor Pathway Inhibitor

Hemostasis is a state in which vascular integrity is maintained without excessive bleeding or clotting. To achieve hemostasis, there are many regulators of the coagulation cascade. One of the main regulators of the extrinsic pathway is the tissue factor pathway inhibitor (TFPI). TFPI is a glycoprotein with a size of 40 kilodaltons (kDa). It is produced within the endothelium and contains three Kunitz domains that facilitate the inactivation of the tissue factor pathway (Broze & Girard, 2012). Kunitz Domain 1 (KD1) interacts with FVIIa-TF, Kunitz Domain 2 (KD2) acts on FXa, and Kunitz Domain 3 (KD3) is believed to have a heparin-binding site. TFPI exerts its anticoagulant function by KD2 binding and inhibiting FXa. Afterward, KD1 binds to TF-FVIIa creating a quaternary complex FXa–TFPI– FVIIa-TF, thereby hindering both FVIIa and FXa function (Wood et al., 2014).

1.1.2.2 Tissue Factor Pathway Inhibitor Isoforms

As a result of alternative splicing, TFPI exists in two isoforms: TFPIα and TFPIβ. Both isoforms carry out similar functions but differ in structure and cellular localization. The most common isoform is TFPIα, found in tissues, endothelial cells, and plasma. This isoform has an acidic N-terminus, KD1 and KD2. Unlike TFPIβ, TFPIα has a KD3 that contains a basic C-terminus (Maroney & Mast, 2015). The function of KD3 is not well established, however studies indicate that KD3 has a binding site for heparin and Protein S (PS). Thus, it is believed that TFPIα has a secondary function, which is to inhibit the prothrombinase complex (Wood et al., 2014).

TFPIα truncation produces TFPIβ that lacks the acidic N-terminus and KD3. It is mainly found in endothelial cells and platelets. TFPIβ is released and circulates freely in the plasma. TFPIβ has KD1, KD2, and a glycosylphosphatidylinositol (GPI) C-terminus. GPI anchors the protein to the cell membrane and strengthens FXa inactivation. Both isoforms can be subjected

to post-translational modifications, which impact their function and localization (Wood et al., 2014). Taken together, both TFPI types reduce the availability of FVIIa and FXa in the blood, which impedes thrombin generation. Overall, hemostasis works towards balancing the procoagulant and anticoagulant processes. TFPI along with other natural anticoagulants (activated protein C, antithrombin) and procoagulants (activated coagulation factors) help prevent pathological bleeding and clotting (Dorgalaleh et al., 2018).

1.1.2.3 Clearance of Tissue Factor Pathway Inhibitor

The method by which the body eliminates TFPI from the bloodstream is via lysosomal degradation. TFPI recognizes and binds to ligand-binding domains on Lipoprotein receptor-related protein 1 (LRP1), leading to LRP1-TFPI complex formation and internalization (Narita et al., 1995). The complex is then transported through the endocytic pathway and sent to the lysosomes for degradation. Lysosomes are acidic organelles containing various hydrolytic enzymes and proteases. Within the lysosomes, TFPI is degraded by these proteases, resulting in its breakdown into smaller peptides and amino acids (He et al., 2021).

1.1.3 Contact pathway

The contact pathway is also referred to as the intrinsic pathway. It is called the contact pathway because it is triggered by contact with negatively charged surfaces, as previously described. The negatively charged surfaces promote the autoactivation of FXII, then FXIIa proteolytically cleaves prekallikrein (PreK) to plasma kallikrein (PK) (Wu, 2015). In turn, PK exhibits a positive feedback loop and cleaves FXII to FXIIa. Consequently, the contact pathway diverges and initiates the kinin system and coagulation cascade (Figure 2). This is accomplished when PK produces HMWK, releasing bradykinin, while FXIIa activates FXIa to induce thrombin generation via the common pathway (Campbell, 2001).

1.1.4 Kallikrein-kinin system

The kallikrein-kinin system is a multifaceted cascade incorporating various biochemical reactions. As presented in Figure 2, key components of this pathway are kallikreins, kininogens, and kinin receptors. Kininogen is a plasma glycoprotein synthesized primarily in the liver (Costa-Neto et al., 2008). Like TFPI, it exists in two isoforms: high molecular weight (HMWK) kininogen and low molecular weight (LMWK) kininogen. As a cofactor, HMWK aids the coagulation pathway by facilitating the cleavage of FXI and FXII (Ponczek, 2021). It also helps modulate blood pressure. Once cleaved by plasma kallikrein, it releases bradykinin (BK), a potent vasodilator, and reduces blood pressure (Kayashima et al., 2012). Bradykinin promotes smooth muscle relaxation and increases blood vessel diameter. The second kininogen isoform is LMWK, a smaller protein that functions by producing a BK precursor or kallidin (Moreau et. al, 2005).

Alternative splicing of *KNG1*, the kininogen gene, produces two isoforms. Proteins differ at the C-terminus; HMWK is the full-length isoform with 626 amino acids and comprises six domains (D). D1 has a low affinity for calcium, D2 acts on the endothelial cell receptor C1q, D3 on platelets, D4 contains the BK sequences, and D5 is the histidine-rich domain that binds to negatively charged surfaces. The region that contributes to the contact pathway is the C-terminus of D6; it interacts with FXI and PK (Pathak et al., 2013). In contrast, LMWK has 409 amino acids and does not carry a sixth domain. It acts as a substrate for tissue kallikrein (TK).

1.1.5 Kallikrein

Kallikreins are serine proteases that cleave kininogens, leading to the production of vasoactive peptides called kinins. Different kallikrein types are expressed in different tissues and have distinct roles. The two kinds of kallikreins are plasma and tissue kallikrein. Plasma kallikrein (PK) is a protease encoded by *the KLKB1* gene on chromosome 4 q34-35 with a

molecular weight of 86 kDa. It is predominantly produced in the liver and plays a significant role in the coagulation cascade, specifically in the intrinsic/contact pathway (Moreau et. al, 2005). PK is produced when FXIIa cleaves its precursor, prekallikrein. Next, PK cleaves HMWK to produce LMWK and a peptide, BK. As discussed, BK stimulates blood vessel dilation and permeability. This effect is achieved by binding to the B2 receptor (B2R), a G-coupled receptor that induces endothelial cell contraction, vasodilatation, and nitric oxide production (Maas et al., 2011). Subsequently, fluid and immune cells extravasate into peripheral tissues, triggering inflammation and immune responses (De Maat et al., 2018).

Tissue kallikreins comprise a group of fifteen closely related proteases encoded by the *KLK* gene cluster on chromosome 19 q13.2 – q13.4, all with a molecular weight of 30 kDa (Kalinska et al., 2016). They are primarily expressed in tissues, such as the pancreas, spleen, and kidneys (Moreau et. al, 2005). TK cleaves LMWK to Kallidin, a decapeptide with an added lysine residue at the N-terminus. Kallidin can be converted to BK by an aminopeptidase. If not converted to BK, Kininase I cleaves Kallidin, which then binds to the B1 receptor (B1R). As B2R, B1R is a G-coupled receptor on endothelial cells that promotes fluid accumulation in the vasculature (Yousef & Diamandis, 2001).

1.2 Hereditary Angioedema

1.2.1 Prevalence

Hereditary angioedema (HAE) is a rare autosomal dominant disease that results in spontaneous swelling due to increased vascular permeability. Typically, fluids accumulate in the deeper layers of the skin or mucosal tissues. Symptoms include swelling of the face, extremities, and larynx. Laryngeal edema is the most feared symptom, as it can lead to asphyxiation. Approximately 1 in 10,000 to 50,000 persons have HAE. Usually, patients have one to three attacks per month, and each can last 2 to 3 days (Cicardi, 2010).

1.2.2 Pathology and Genetics

The mechanism responsible for manifesting this condition is the contact pathway, specifically the under-regulation of this pathway. As illustrated, the contact pathway involves the autoactivation of FXII, which then cleaves PreK to PK. PK presents a positive feedback loop and activates FXII. Thereafter, FXIIa initiates coagulation, whereas PK stimulates the kinin system and produces BK (Campbell, 2001). Subsequently, uncontrolled BK levels result in fluid accumulation in peripheral tissues and inflammation (De Maat et al., 2018).

The primary cause of HAE is C1-esterase inhibitor (C1INH) deficiency. C1INH is a serine protease inhibitor (serpin) with a molecular weight of 110 kDa. It is encoded by the *SERPING1* gene on chromosome 11 (11q12.q13.1). C1INH regulates vascular permeability by inhibiting activated Factor (FXIIa) and plasma kallikrein (PK) (Björkqvist et al., 2013). It is responsible for 93% of FXIIa and 52% of PK inactivation in human plasma (De Maat et al., 2018). Normally, C1INH prevents the excessive production of BK by inactivating PK, but HAE patients exhibit elevated levels of BK due to C1INH deficiency or dysfunction (Nzeako et al., 2001).

HAE is subdivided into three distinct subtypes: type 1, type 2, and the more recently acknowledged type 3. Type 1 exhibits quantitative C1INH deficiency, while type 2 displays C1INH dysfunction. Both types are a result of *SERPING1* abnormalities (Zuraw, 2018). Type 1 arises from deletion mutations, while type 2 arises from substitution mutations (Riedl, 2013). Furthermore, type 3 is characterized by normal C1INH levels and function and no mutations within the *SERPING1* gene; instead, a missense mutation is detected in the FXII gene. Studies indicate that type 3 is exclusively present in females as it is believed to be linked to estrogen fluctuations. The mechanism of type 3 is not well identified; however, it is understood that

changes in estrogen levels induce FXII production leading to overactivation of the contact pathway and BK release (Cichon et al., 2006).

1.2.3 Triggers and Diagnosis

Triggers for HAE attacks vary from person to person, but common triggers include hormonal fluctuations due to pregnancies or menopause, infections, allergies, and stresses. Stresses refer to both emotional and physical stresses. Physical stress could arise from injuries or surgeries, causing bleeding and contact pathway stimulation. Additionally, some medications, such as angiotensin-converting enzyme (ACE) inhibitors, promote bradykinin production and vascular permeability (Bernstein, 2018).

To diagnose patients with HAE, physicians perform clinical evaluations, history assessments, and laboratory tests. First, professionals will inspect for unexplained swelling of the limbs, face, abdomen, or genitals. Next, blood samples are obtained to determine C1INH levels and functionality. Physicians also assess the levels of complement factor 1 and factor 4, as they are regulated by C1INH (Poppelaars et al., 2016). Less commonly, genetic testing is conducted to detect *SERPING1* gene abnormalities (Bernstein, 2018).

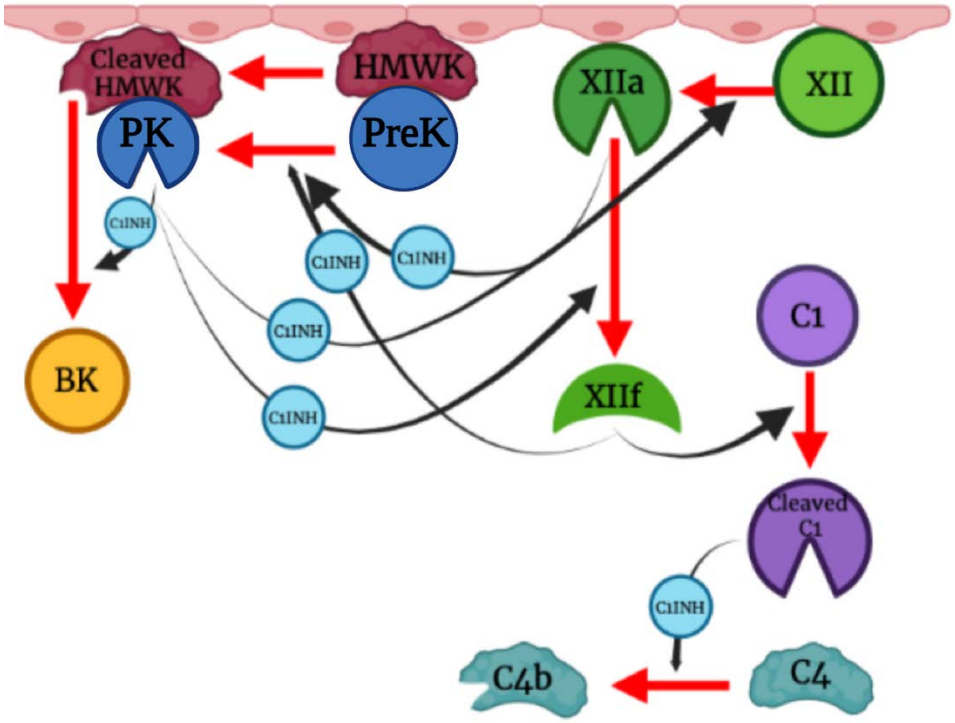

Figure 2: **The contact pathway and its regulation by C1INH.** Black and red arrows represent cleavage, and regulation by C1INH, respectively. FXII: Factor XII, FXIIa: activate Factor XII, PK: Plasma Kallikrein, C1: complement cofactor 4, C4: complement cofactor 4, C1INH: C1 esterase inhibitor, HMWK: High Molecular Weight Kininogen, PreK: Prekallikrein, BK: Bradykinin.

1.2.4 Existing treatments

1.2.4.1 Agents Treating Acute HAE Attacks

There are various treatments available for acute HAE attacks, including Berotralstat, Icatibant, and Ruconest (Lee, 2021). Berotralstat is an oral agent that inhibits PK and has a life span of 93 hours. Unfortunately, it costs $38,959 for a 28-day supply and has been associated with gastrointestinal side effects (Powell et. al, 2022). Moreover, Ruconest is a recombinant C1INH produced in the milk of transgenic rabbits, thus comes with immunogenic concerns (Cruz, 2015). Icatibant is a synthetic decapeptide that acts as a B2R antagonist by mimicking the structure of BK. Like Ecallantide, it has a very short half-life ($t_{1/2}$= 2 hours) (Riedl, 2010). Existing drugs have demonstrated effectiveness at treating acute HAE attacks; however, they are either extremely expensive or have short half-lives.

1.2.4.2 Agents for Prophylactic Use

Currently, physicians are working towards prophylactic rather than on-demand treatment; a drug approved for prophylactic application is Lanadelumab. Lanadelumab is a monoclonal antibody that inactivates PK and has a half-life of 2 weeks. It has proven to be effective, but it costs 48,908 USD for a 28-day supply and may be associated with upper respiratory infections (Hahn et. al, 2020). Additionally, subcutaneous CINH injections have been shown to be successful at treating and preventing HAE attacks (Longhurst et al., 2017). Similar to Lanadelumab, C1INH injections are extremely expensive. Providing patients with C1INH accounts for 13% of the Canadian Blood Services (CBS) budget. In 2018, CBS dedicated 125 million CAD to deliver C1INH injections to Canadian patients (Canadian Blood Services, 2019). Overall, fewer drugs are indicated for HAE prophylaxis than HAE acute treatment (Nzeako, 2001). Therefore, it is necessary to develop medications that are feasible and enable prophylactic application.

1.3 Protein clearance

1.3.1 Protein synthesis, secretion, and clearance

Protein synthesis is the process of transcribing and translating genes to produce proteins. Protein synthesis and secretion incorporate the production, modification, and transportation of proteins to their final destinations to perform their functions. Proteins come in different structures and sizes. It is widely known that structure dictates function. Similarly, protein modifications by subcellular organelles such as the endoplasmic reticulum (ER) play a role in proteins' function and location (Moldave, 1985).

To maintain equilibrium between protein synthesis and degradation in the body, proteins undergo clearance. This process facilitates protein renewal and eliminates the accumulation of harmful or malfunctioning proteins. Protein turnover rates vary depending on their function and destination. Various organs and systems aid protein clearance, including the kidneys, liver, and immune system. The kidneys filter out small proteins circulating in the body. Proteins that fall below the glomerular filtration limit and are not reabsorbed in the proximal tubules are excreted in the urine (Ferguson & Waikar, 2012). In contrast, the liver metabolizes proteins through endocytosis, a receptor-mediated uptake that typically leads to protein degradation (Xia et al., 2020). Additionally, the immune system removes expired or foreign proteins through macrophages, which engulf and degrade their targets (Gordon, 2007). Protein catabolism is a process that breaks proteins into their respective amino acids (Callis, 1995). This mechanism is valuable as it enables amino acid recycling for new protein synthesis, removing potentially damaged proteins, and balancing protein levels (Martinez-Vicente et al., 2005).

1.3.2 Clearance receptors

1.3.2.1 Neonatal Fc receptor

The neonatal Fc receptor (FcRn) is a protein composed of two subunits, making it a heterodimer glycoprotein. It contains α1-α2-α3 domains, a transmembrane glycoprotein, and a β2-microglobulin subunit. The α-chains, transmembrane glycoprotein, and cytoplasmic tail make the FcRn heavy chain (FcRnHC) and the β2-microglobulin subunit makes the light chain. FcRn is mainly synthesized in endothelial cells and antigen-presenting cells (Latvala et al., 2017). FcRn has numerous functions, including recycling and transporting immunoglobulin G (IgG) antibodies and albumin (Oganesyan et al., 2014). As in Figure 3, the recycling begins with the Fc portion of IgG binding to FcRn. The binding is pH-dependent; at neutral pH conditions, FcRn and IgG are engulfed via receptor-mediated endocytosis. Under acidic pH conditions in the endosomes, FcRn binds to Fc, forming a stable FcRn-Fc complex that saves IgG from lysosomal degradation. Low pH is crucial as it results in FcRn conformational change, enhancing its affinity for IgG. The binding is due to interactions between the histidine residues in the CH2–CH3 hinge region of IgG and acidic residues on the FcRnHC (Pyzik, et al., 2023). IgG that fails to bind FcRn is catabolized via lysosomal degradation. IgG recycling is important as it saves and transfers maternal IgG to newborns and regulates antibody levels in the body (Roopenian & Akilesh, 2007). Similarly, FcRn binds to albumin and rescues it from degradation. Albumin binds to FcRnHC in an interaction involving three conserved histidine residues on domain III of albumin. Overall, FcRn prolongs the circulatory life span of both IgG and albumin (Kuo et al., 2010).

1.3.2.2 Low-density lipoprotein receptor-related protein 1

Low-density lipoprotein receptor-related protein 1 (LRP1) is a receptor found in hepatocytes that plays a fundamental role in maintaining cellular homeostasis. It is a member of the low-density lipoprotein (LDL) receptor family that reinforces protein catabolism via internalization and degradation. This effect is achieved by recognizing and engulfing ligands (He et al., 2021). LRP1 carries a modular structure composed of clusters of cysteine-rich complement-type repeats (CR). CR domains act as binding sites for ligands. LRP1 binds ligands via salt bridges between lysine residues on the ligand and carboxylates of aspartate residues within CR (Lillis et al., 2008). As described, LRP1 is responsible for degrading TFPI; it internalizes TFPI and mediates its lysosomal degradation. This process is critical as it regulates TFPI levels and coagulation processes. To further regulate coagulation, LRP1 participates in clearing various proteins including α2-Macroglobulin (α2M), serpin-enzyme complexes, and FVIIIa (Strickland, 2014).

1.4 Half-life extension technology

1.4.1 Genetic fusion to Albumin or Fc domains

As mentioned, the prophylactic application is gaining more interest within healthcare, hence it is necessary for drugs to have a long-lasting therapeutic impact. Half-life extension technology employs techniques designed to elongate the half-life of drugs. A drug's half-life is the duration between the administration and the elimination of half of the dose from the body (Toutain & Bousquet-mélou, 2004). A drug could be removed from circulation via degradation, filtration, or metabolism. By extending the half-life, a medication's period of action is amplified, thereby enhancing its efficacy. A common strategy applied is genetic fusion to human serum albumin or to the Fc domain of IgG. Typically, small proteins are fused to HSA or Fc domain to enforce protein recycling and to resist filtration via the kidneys (Strohl, 2015).

Albumin is the most abundant large protein in the body. It is synthesized in the liver and has a half-life of 19 days. Human serum albumin has a molecular weight of 66 kDa and carries out various functions. It controls plasma pH, transports metabolite and fatty acids, and regulates blood pressure. Albumin exceeds the glomerular filtration limit, and its clearance is governed by recycling via the ubiquitous FcRn receptor (Sleep, 2013). Previous recombinant proteins fused with HSA in the Sheffield lab include barbourin-HSA (Marques et al., 2001), hirudin-HSA (Syed et al., 1997), and Kunitz Protease Inhibitor-HSA (KPI-HSA) (Sheffield et. al, 2018). In comparison to unfused barbourin/ hirudin/ KPI, fusion proteins presented half-life extensions in CD-1 mice. Additionally, coagulation proteases, such as FIX, have been fused with albumin and demonstrated half-life elongation and function preservation (Sheffield et al., 2004, Schulte, 2009).

Immunoglobulin G (IgG) is an antibody isotype that significantly contributes to the immune system. It is the most abundant antibody class in the circulation and is responsible for various processes, such as neutralizing pathogens, opsonizing, and activating cellular pathways in response to harmful material. It has a long half-life of 21 days. Its long half-life is due to the interaction between the constant region of IgG, Fc domain, with FcRn. Thus, genetically introducing Fc domains to therapeutic proteins serves similar benefits as HSA-fusions. Studies suggest that Fc has been successful at extending various protein half-lives, including those of FIX, growth factors and cytokines (Kontermann, 2011).

Genetic fusion refers to the construction of sequences that incorporate the desired therapeutic protein combined with an Fc or HSA domain. This allows the protein to piggyback on the long lifespan of HSA or IgG. Both kinds of genetic fusions come with numerous advantages. Fc fusions help solubilize hydrophobic proteins and promote binding to multiple

ligands due to their bivalent nature (Smales & James, 2008). Depending on the Fc isotype, it could also provide secondary cytotoxic functions. As for HSA fusions, HSA is present in high concentrations in plasma and is efficiently produced in yeast expression systems. In comparison to Fc fusion proteins, only monomeric fusions are created, so purification is simplified. Also, it does not carry a secondary function; thus, therapeutic requirements must be established prior to selecting the half-life extension technology (Smales & James, 2008). Regardless, both methods improve drugs' efficacy and decrease the dosing frequency, therefore making them valuable tools in biopharmaceutical development.

1.4.2 Non-covalent binding to Albumin

Furthermore, recent studies have presented promising results surrounding albumin domains deriving complex formations with albumin. A binding domain investigated in literature is Albumin Binding Domain 035 (ABD). It is a 46 amino acid three-helical albumin binding domain found in surface proteins of gram-positive bacteria (Guo, 2016). Genetically fusing small proteins with ABD could promote non-covalent binding to endogenous human and mouse serum albumin (Frejd, 2012). ABD can bind to more than one albumin and partake in FcRn recycling. Reportedly, ABD has a high affinity for HSA, with an equilibrium dissociation constant (K_D) of 120 fM (Nilvebrant & Hober, 2013). Therefore, it is believed that fusing small proteins with ABD will induce the ABD fusion protein to adopt some of albumin's properties, including undergoing recycling leading to half-life elongation.

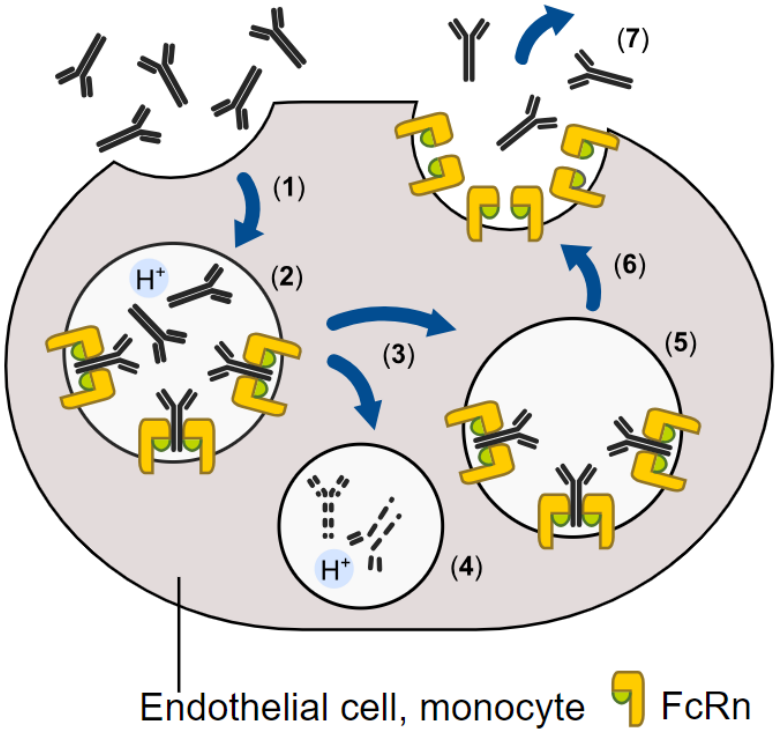

Figure 3: Albumin recycling via the FcRn pathway. At neutral pH, IgG (y-shaped molecule) or albumin or IgG or albumin fusion proteins are internalized by endothelial cells or monocytes via pinocytosis (step 1). A decrease in the pH in endosomes promotes IgG/albumin binding to FcRn (yellow/green molecule) (step 2). Molecules that fail to interact with FcRn are sent to the lysosomes for degradation (steps 3 and 4). Vesicles carrying IgG/albumin–FcRn complexes are protected from degradation (step 5) and redirected to the cell surface (step 6). Transport vesicle fusion to the plasma membrane exposes IgG/albumin-FcRn to neutral pH and IgG/albumin is released back into the bloodstream (Image source: https://commons.wikimedia.org/wiki/File:FcRn_mechanism_of_inhibition-en.svg reproduced with permission under the Creative Commons Attribution-Share Alike 4.0 International license).

1.4.3 Chemical modification

Another strategy applied to achieve half-life extension is chemical modification. Chemical modification provides proteins with stability and shielding from degradation and filtration. This effect is possible by covalently attaching chemical groups such as polyethylene glycol (PEG) chains to the primary amines or sulfhydryl groups found in the protein of interest (Tully et al., 2021). The hydrophilic property of PEG increases proteins' solubility and enlarges the hydrodynamic size, thus evading glomerular filtration and facilitating their remaining in the bloodstream for extended periods (D'souza & Shegokar, 2016). For instance, FVIII modified with PEG demonstrated half-life extension and clinical efficacy (Mannuccio, 2015) (Tiede, 2015) and several pegylated recombinant FVIII products are currently in clinical use in Canada (Canadian Blood Services, 2022). Overall, the half-life extension method of choice depends on various factors, including the size of the drug, pharmacokinetic properties, therapeutic goal, and target location. Ultimately, the aim is to present a long-lasting restorative impact while limiting potential side effects.

1.5 Ecallantide

Ecallantide (KalbitorTM) is an engineered variant of Tissue Factor Pathway Inhibitor (TFPI), a plasma protein that impedes the activation of the extrinsic pathway within the coagulation cascade. When bound to tissue factor, TFPI inhibits Factor Xa and VIIa (Wood et. al, 2014). Ecallantide is comprised of the first Kunitz domain of TFPI. Recombinant Ecallantide (rEcall) was selected by phage display and has seven amino acid substitutions reported to make it specific for PK inhibition (Garnock-Jones, 2010). rEcall has an apparent weight of 7 kDa and contains 60 amino acids. It functions by reversibly binding and blocking the active site of plasma kallikrein. In the United States, ecallantide is FDA-approved for treating acute HAE attacks in

patients aged ≥ 12 years. Typically, 30 mg of ecallantide is subcutaneously administered. It has a half-life of two hours, thus precluding prophylactic application (Lunn, Duffey & Firszt, 2015). Therefore, we aimed to empower the prophylactic use of rEcall by extending its life span. The half-life extension technology utilized was a genetic fusion of rEcall to human serum albumin (HSA) or an albumin binding domain (ABD). It was anticipated that fusing rEcall with HSA or ABD would prolong rEcall's half-life while maintaining its primary function.

1.6 Expression system

Pichia pastoris is a methylotrophic yeast that functions as a biological expression system. *Pichia pastoris* was chosen to express rEcall proteins because clinical trials showed that HSA made in this system behaved indistinguishably from plasma-derived HSA (Kobayashi, 2006). Moreover, clinical rEcall is produced in this system (Zuraw et. al, 2010). *Pichia pastoris* has various advantages; it is inexpensive, has a defined protocol, and produces a high yield of recombinant proteins secreted directly into the supernatant of the culture medium (Karbalaei, 2020).

1.7 Rationale

Patients suffering from C1INH deficiency or dysfunction have been shown to exhibit life-threatening symptoms, such as asphyxiation, due to the overproduction of BK. There are unmet clinical needs for a therapy that will modulate PK activity for extended periods. This is crucial because pharmaceutical companies lack an HAE drug that is effective, inexpensive, and approved for prophylaxis. As illustrated, Ecallantide is an FDA-approved drug that is used for acute HAE attacks. Its short half-life precludes prophylactic application. Previously, albumin fusion proteins have been successful at elongating proteins' life spans and retaining their integral function. To assess albumin fusion as a potential strategy to extend rEcall half-life, rEcall

recombinant proteins with HSA fused at the N- or C-terminus were genetically engineered and expressed in *Pichia pastoris*. Thereafter, proteins were purified to facilitate activity and clearance experimentations.

1.8 Hypothesis

Albumin fusion/binding will extend the circulatory half-life of ecallantide without impairing PK inhibition.

1.9 Objectives

The objectives of this study were to compare *in vitro* inhibitory properties and *in vivo* pharmacokinetics of *P.pastoris* derived recombinant rEcall proteins. These objectives involved expressing H_6-rEcall, rEcall-H_6, H_6-rEcall-ABD, H_6-rEcall-HSA, and HSA-rEcall-H_6 in *P.pastoris* via the yeast prepro-α factor secretory signal sequence, purifying via Nickel Affinity Chromatography, assessing activity by determining kinetic parameters, and comparing their pharmacokinetics in mice.

2.0 Methods

2.1 Constructs:

The pPICZamp9ss vector (pZAMP), created in the Sheffield laboratory, was used to create rEcall expression plasmids (Sheffield et al., 2005). This vector combined an ampicillin resistance gene for plasmid selection, a Sh ble Zeocin resistance gene for yeast transformation, an origin of replication, and an Alcohol Oxidase 1 (AOX1) methanol-inducible promoter. The Ampicillin resistance gene was introduced so that plasmid DNA manipulation in bacteria could be performed using a less expensive antibiotic than Zeocin for a part of the process. The vector also included a cleavable yeast prepro-α factor secretory signal sequence and was modified to contain an N- or C-terminal hexahistidine tag (H_6-tag). The H_6-tag was incorporated for purification purposes.

As shown in Table 1, to create the desired constructs, commercial gene synthesis (gBlocks™, Integrated DNA Technologies IDT) was used to build H_6-rEcall, ABD, and HSA cDNAs. gBlocks are double-stranded DNA gene fragments of up to 3000 bp in length. The gBlocks™ also included a 15-codon glycine– serine repeat $(G4S)_3$ linker to separate and create a buffer zone between rEcall and ABD or HSA domains. The linker decreases the chance of steric hindrance in PK–rEcall binding (van Rosmalen, 2017). However, the GC-rich nature of the linker prevented simple integration into one gBlock. Thus, two gBlocks were employed per fusion construct.

As shown in Figure 1, the full list of recombinant proteins expressed in this study also included rEcall-H_6 and HSA-rEcall-H_6. These additional constructs were required for a systematic study of the relative position of H_6 tags and HSA fusion domains on rEcall activity.

The order of the components comprising each recombinant protein employed in this study is illustrated in Figure 4, which also provides the predicted number of amino acids for each construct after synthesis in *Pichia pastoris* X-33 yeast and secretion into the conditioned media.

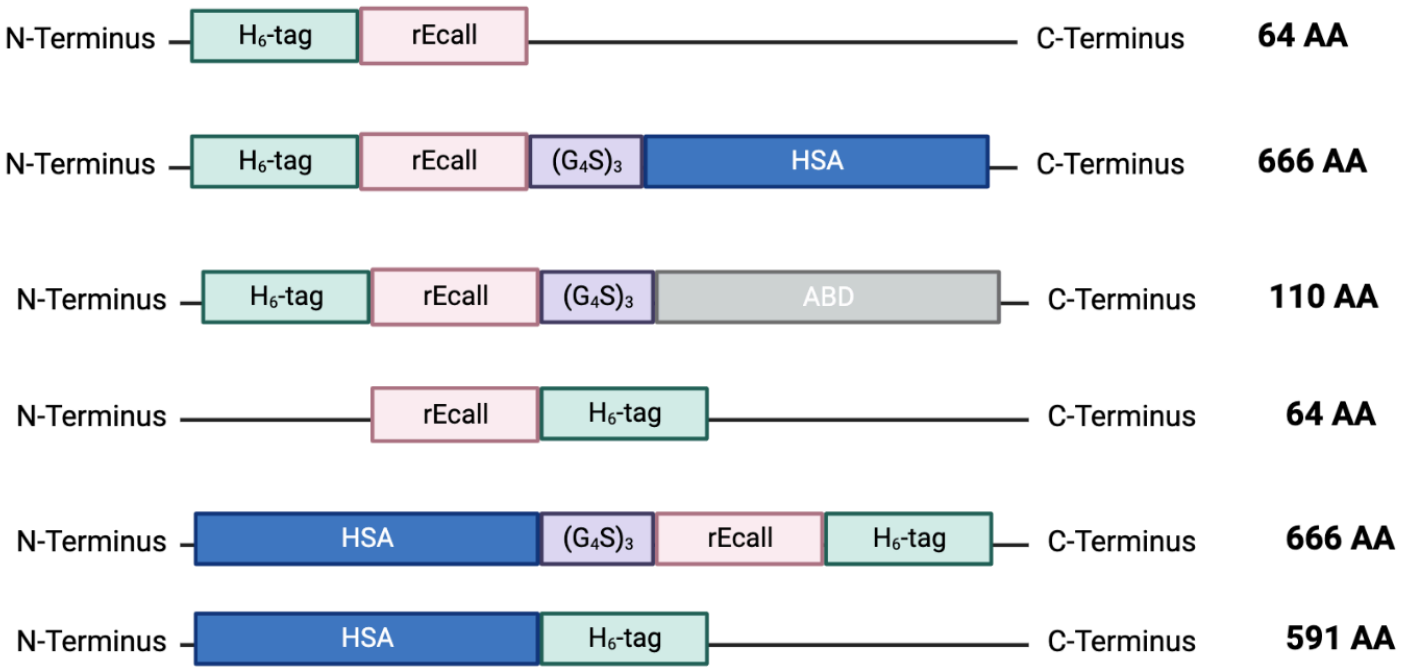

Figure 4: Schematic diagram of constructed plasmids, displayed in a linear form. Plasmids were H_6-rEcall, H_6-rEcall-ABD, H_6-rEcall-HSA, rEcall-H_6, HSA-rEcall-H_6, and HSA-H_6. Green boxes represent the position of H_6-tag, pink boxes are rEcall residues, purple boxes are $(G4S)_3$ linker, the grey box is ABD, and blue boxes are HSA residues. Length of proteins in amino acids (AA) is indicated at right.

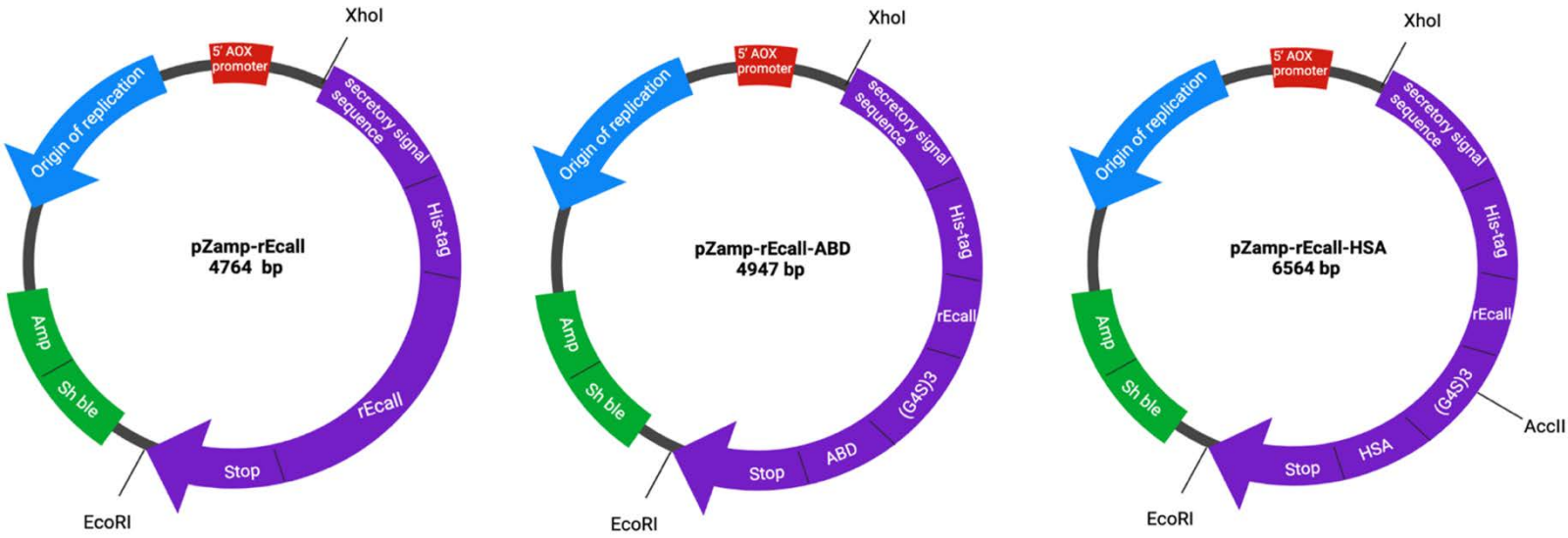

Figure 5a: Schematic diagram of expression plasmids. The relative position and identity of genetic components of three double-stranded DNA expression plasmids identified, with names and their size in base pairs given centrally, is shown. The elements include: origin of replication; 5' alcohol oxidase promoter (5' AOX promoter); secretory signal sequence (from pre-pro alpha factor; H_6-tag; rEcall codons; linker codons $((G4S)_3)$; Albumin Binding Domain codons (ABD); Human Serum Albumin codons (HSA); translational and transcriptional termination signals (Stop); and dominant selectable markers for ampicillin resistance gene (amp) and zeocin resistance gene (*sh ble*). The position of selected restriction endonuclease sites is shown.

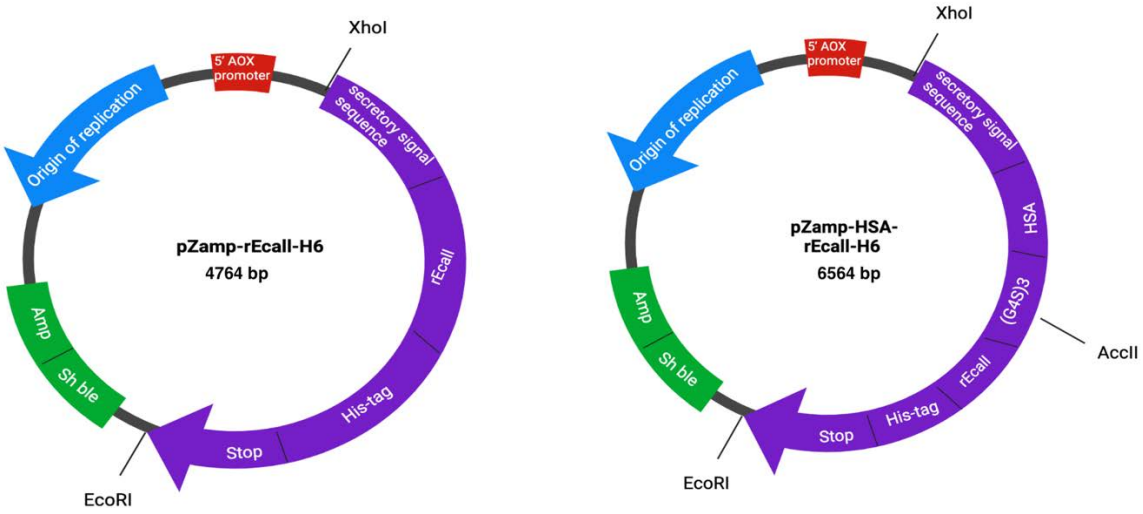

Figure 5b: Schematic diagram of new expression plasmids. The relative position and identity of genetic components of two double-stranded DNA expression plasmids, with names and their size in base pairs given centrally, is shown. Genetic elements are as shown in Figure 5a.

As illustrated in Figure 5, all constructs were designed to exploit the AOX1 promoter region, which allows for methanol-inducible protein expression in *Pichia Pastoris*. The yeast secretory signal sequence (yeast prepro-α factor 85) includes a Kex2/Ste13 protease cleavage site (SLEKR↓EA). This site was conserved in our construct design. The secretory signal sequence is crucial as it marks target proteins to be secreted into the conditioned media by passage through the endoplasmic reticulum and the Golgi apparatus. As indicated previously, H_6-tags were employed to facilitate purification and the $(G4S)_3$ linker created a buffer zone between rEcall and HSA or ABD.

2.2 Assembly of construct genetic elements:

2.2.1 pZAMP-H_6-rEcall

The assembly of pZAMP-H_6-rEcall used Geneblock F, comprising 228 nucleotides encoding a XhoI Restriction Enzyme (RE) site at its 5'end, yeast signal sequence, H_6 tag, Ecallantide, stop codon, and an EcoRI RE site at its 3' end. The construct was assembled via a two-part ligation, combining Geneblock F and vector pZAMP, both restricted with XhoI and EcoRI. The final construct encoded by the plasmid arising from the insertion of synthetic DNA (pZAMP-H_6-rEcall) was predicted to be 4764 bp and to result in the expression of a 65 amino acid protein of ~7 kDa.

2.2.2 pZAMP-rEcall-H_6

The assembly of pZAMP-rEcall-H_6 used Polymerase Chain Reaction (PCR)-based mutagenesis. Plasmid pZAMP-H_6-rEcall was used as a template for PCR to generate pZAMP-rEcall-H_6, using heat-stable polymerase Phusion as directed by the manufacturer (Thermo Fisher Scientific, Waltham, MA, USA). The forward oligonucleotide (5' GCATCTCGAG AAAAGGGAAG CGATGCATAG CTTTTGCGCG 3') flanked the unique XhoI restriction site within the secretory sequence while the reverse oligonucleotide (5' GCATGAATTC TCAATGGTGA TGGTGGTGAT GATCGCGGGT GCACAT 3') flanked the EcoRI restriction site downstream of the rEcall termination codon. The 228 bp amplification product (Amplicon 1) was restricted with XhoI and EcoRI and was ligated to XhoI/EcoRI double-digested pZAMP to form pZAMP-H_6-rEcall, in a two-part ligation. The final construct was pZAMP-rEcall-H_6 and had the same size as pZAMP-H_6-rEcall.

2.2.3 pZAMP-H_6-rEcall-ABD

The assembly of pZAMP-H_6-rEcall-ABD used Geneblock F, comprising 409 nucleotides encoding a XhoI restriction endonuclease site at its 5’ end, yeast signal sequence, H_6 tag, Ecallantide, $(G4S)_3$ spacer, ABD cDNA, stop codon, and an EcoRI restriction endonuclease site at its 3’end. The construct required a two-part ligation, joining XhoI- and EcoRI double digested Geneblock H and pZAMP. The final construct encoded by the plasmid arising from the insertion of the synthetic DNA (pZAMP -rEcall-ABD) was predicted to be 4947 bp and to result in expression of a 126 amino acid protein of ~14kDa.

2.2.4 pZAMP-H_6-rEcall-HSA

The assembly of pZAMP-H_6-rEcall-HSA employed two synthetic geneblocks. Geneblock G comprised 252 nucleotides encoding an XhoI restriction endonuclease site at its 5’ end, yeast signal sequence, H_6 tag, Ecallantide and 2/3 portion of a (G4S) linker, and an AccIII restriction endonuclease at its 3’end. Geneblock B consisted of 1792 nucleotides encoding an AccIII restriction endonuclease site at its 5’end, 1/3 portion of (G4S) linker, the entire mature HSA cDNA, stop codon, and an EcoRI restriction endonuclease site at its 3’ end. Geneblock G was digested with Xho I and AccIII and Geneblock B was digested with AccIII and EcoRI, which were ligated with XhoI-EcoRI-restricted pZAMP in a three-part ligation. The final construct encoded by the plasmid arising from the insertion of synthetic DNA (pZAMP-H_6-rEcall-HSA) was estimated to be 6564 bp and to result in the expression of a 665 amino acid protein of ~75kDa.

2.2.5 pZAMP- HSA-rEcall-H_6

The assembly of pZAMP-HSA-rEcall-H_6 used PCR-based mutagenesis. Next, pZAMP-H_6-rEcall-(G4S)3-HSA and pZamp-H_6-rEcall were used as templates in PCR using conditions described above. For the first template, the forward oligonucleotide (5'GCATCTCGAGA AAAGGGACGC TCATAAGTCC 3') flanked the XhoI restriction site within the secretory sequence while the reverse oligonucleotide (5' GCATTCCGGAC CCACCGCCAC CACTTCCACC TCCGCCCAGG CCTAAGGCTGC 3') flanked $(G_4S)_3$ codons at the C-terminus. For the second template, the forward oligonucleotide (5' GCATCTCGAGA AAAGGGACGC TCATAAGTCC 3') flanked the $(G_4S)_3$ codons while the reverse oligonucleotide (5' GCATTCCGGA CCCACCGCCAC CCACTTCCAC CTCCGCCCAGG CCCAGGCCTAA GGCTGC 3') flanked rEcall codons at the C-terminus. Separate PCR generated two amplicons, Amplicons 2 and 3 respectively. Restriction of Amplicon 2 with XhoI and AccIII and of Amplicon 3 with AccIII and EcoRI, which were inserted between the XhoI and EcoRI sites of pZAMP in a three-part ligation. The final construct encoded by the plasmid arising from the insertion of PCR-amplified DNA (pZAMP-HSA-rEcall-H_6) had the same size and properties as C-terminally HSA-tagged rEcall.

Table 1 summarized the DNA elements used to assemble all constructs described in detail above.

Table 1: Geneblocks with their respective RE sites and sizes.

DNA elements	Name	Size (bp)	RE sites
gBlock F	H_6-rEcall	228	XhoI, EcoRI
gBlock G	H_6-rEcall-(G4S)2	252	XhoI, AccIII
gBlock B	G4S-HSA	1776	AccIII and EcoRI
gBlock H	H_6-rEcall-ABD	409	XhoI, EcoRI
Amplicon 1	rEcall-H_6	228	XhoI, EcoRI
Amplicon 2	HSA-(G4S)	1776	XhoI, AccIII
Amplicon 3	$(G4S)_2$-rEcall-H_6	252	AccIII and EcoRI
pPICZamp9ss	pZAMP	4554	XhoI and EcoRI

2. 3 Digestion, ligation, and transformation of DNA into *Escherichia coli* TOP10:

The cDNAs were subjected to standard methods of DNA digestion, ligation, transformation of *E. coli* TOP10 cells to ampicillin resistance, characterization of plasmid candidates by restriction of plasmid DNA and gel electrophoresis, and validation of selected plasmid DNA candidates by confirmatory Sanger sequencing, as described (Sheffield et al., 2005). For Sanger sequencing, constructs were sent to Mobix Lab within the McMaster Genomics Facility.

2.4 *P. Pastoris* transformation and small-scale expression

Plasmids validated by DNA sequencing were purified, linearized, and used to transform *P. pastoris* X-33 to Zeocin resistance, as previously described (Sheffield, 2005). Plasmids were incubated with *P. pastoris* chemically competent cells and cultured on YPDS/Zeocin (20g/L YPDS and 0.1mg/ml zeocin) plates at 30° C. It took 3-4 days for colonies to grow. Candidate clones were inoculated into YPD/Zeocin to test for methanol-inducible protein secretion for 24, 48, 72, and 96 hours. This was achieved by performing small-scale expressions in 100ml-200ml of BMMY at 30° C. For five consecutive days, 100% methanol was added to 0.5% culture volume every 24 hours to replenish methanol levels and provide continuous gene induction.

2.5 Nickel chromatography and dialysis:

Nickel-Nitriloacetic acid (Ni-NTA) agarose (Qiagen, Chatsworth, CA, USA) nickel affinity chromatography was used to purify media produced in small and large-scale expression experiments, as described (Sheffield, 2009). To ensure proteins adhered to the resin, conditioned media was neutralized by adding equilibration buffer (50mM Na_3PO_4, 150 mM NaCl, pH = 7.4). Purity was assessed by Sodium Dodecyl Sulphate Polyacrylamide Gel Electrophoresis (SDS-PAGE). Then, gels were stained with Coomassie Brilliant Blue for protein detection. Overnight dialysis was performed at 4°C in 4L of phosphate buffered saline (PBS).

2.6 Concentrating protein preparations

To concentrate the purified sample, Millipore centrifugal concentrators were utilized as directed by the manufacturer (Thermo Fisher Scientific). Purified protein concentrations were determined by measuring optical density at 280 nm using a NanoDrop 2000 spectrophotometer (Thermo Fisher Scientific). The OD reading was then used to calculate the extinction coefficient. The calculation was based on each protein's content of tyrosine, tryptophan, and cystine residues, as described (Gill & Von Hippel, 1989). To further confirm the protein concentration, Bradford assays were performed as described (Bradford, 1976).

2.7 Large-scale expression

The highest expressing subclones were selected for large-scale protein expression in batches of up to 3L culture volume. Methods used in large-scale expressions were analogous to small-scale expressions (Sheffield, 2005).

2.8 Visualizing proteins on a SDS PAGE

A 1 µg aliquot of all recombinant proteins was denatured and electrophoresed on SDS gels, as described above. The small proteins (rEcall-H_6, H_6-rEcall, and H_6-rEcall-ABD) were electrophoresed on a 15% SDS polyacrylamide gel, whereas H_6-rEcall-HSA and HSA-rEcall-H_6 were electrophoresed on a 10% polyacrylamide gel.

2.9 Immunoblotting

To further detect albumin fusion proteins, proteins were electrophoresed on a 10% SDS PAGE and transferred to an Immobilon membrane (Thermo Scientific Pierce). The blot was then blocked overnight with blocking buffer (5% w/vol skim milk in tris-buffered saline with tween-

20, TBST). Next, proteins were immunoblotted with biotinylated-rabbit-anti-hexahistidine antibody (diluted 1µl:20ml in blocking buffer) for 1.5h and followed by a Peroxidase-conjugated Streptavidin (diluted 1ul:20ml in 1% BSA in TBST) for 1h. Thereafter, blots were washed by TBST and visualized using 1:2 enhanced luminol-based chemiluminescent (ECL) (Thermo Scientific Pierce). To image the blot Azure 300 Gel Imaging System was utilized (Azure Biosystems).

2.10 Chromogenic assay

All chromogenic assays conducted in this study were performed on a 96-well microtiter plate at 37°C in PPNE kinetic buffer. PK activity was measured by the velocity of chromogenic substrate S2302 (Diapharma) amidolysis. Velocity was measured in the presence or absence of H_6-rEcall, H_6-rEcall-ABD, H_6-rEcall-HSA, rEcall-H_6, or HSA-rEcall-H_6. In these experiments, 1 nM PK reacted with 0-50 nM of engineered proteins. Next, 0-3200 µM chromogenic substrates were added. Over 5 minutes of observation, the rate of substrate amidolysis was determined using an ELx808 Absorbance Microplate Reader (Biotek). Assays were used as a method of deriving the inhibition constant (K_i).

2.11 Kinetic analysis

The inhibitory constant K_i was determined by linear regression of Lineweaver-Burke plots using GraphPad Prism (GraphPad). For K_i determinations, 1 nM PK reacted with 0–50 nM rEcall proteins. The S2302 concentration varied from 0 to 3200 µM, as described (Sheffield et al., 2018).

2.12 Cleavage inhibition assays

rEcall proteins inhibiting the cleavage of high molecular weight kininogen (HK), FXII, and FIX by PK: To hinder HK cleavage, 100 nM PK was incubated with 1 µM HK and 500 nM rEcall proteins at 37 °C for up to 60 mins. For FXII cleavage inactivation, 1 µM PK was incubated with 2 µM FXII and 2 µM engineered proteins at 37 °C for up to 120 mins. Lastly, for FIX cleavage inhibition, 1 µM PK was incubated with 2 µM FIX and 2 µM engineered proteins at 37 °C for up to 120 mins. FIX-PK reactions included 5 mM $CaCl_2$. Reactions were stopped by adding 4X Sodium Dodecyl Sulphate (SDS) buffer and boiling for 2 min at 95 °C. Samples were assessed by SDS-PAGE and stained with Coomassie Brilliant Blue for protein detection.

2.13 Partial Cleavage assays

Partial cleavage of HK, FXII, and FIX by PK: Conditions were adjusted so that protein cleavage was partial, to increase the ease of detecting inhibition. To partially cleave HK, 100 nM PK was incubated with 1 µM HK and 500 nM rEcall at 37 °C for up to 15 mins. To cleave FXII, 1 µM PK was incubated with 2 µM FXII and 1 µM engineered proteins at 37 °C for up to 40 mins. To cleave FIX, 1 µM PK was incubated with 2 µM FIX and 1 µM engineered proteins at 37 °C for up to 40 mins. FIX-PK reactions included 5 mM $CaCl_2$. Reactions were stopped and electrophoresed, as illustrated above.

2.14 Chromogenic assays incorporating other proteases

To determine the specificity of recombinant proteins for PK, their inhibitory activity against 10 nM PK, 150 nM FXIIa, 10 nM FXIa, 5 nM FIXa, 10 nM FIIa, and 100 nM plasmin (PLSN) was tested. All proteins were diluted in PPNE buffer (20mM Na_3PO_4 pH 7.4, 100mM NaCl, 0.1mM EDTA, 0.1% (w/v) PEG 8000) creating a recombinant protein: protease ratio of 2:1 in each well. 180µl of 100 µM of chromogenic substrates were used (S-2302 for PK/FXIIa/

FIIa, S-2366 for FXIa, S2765 for FXa, and S2251 for PLSN); activity was measured at 37°C. The mean velocity of amidolysis of all wells was collected and compared to PK amidolysis.

2.15 Radiolabelling and *in vivo* clearance in mice

^{125}I-labelled sodium iodide was utilized to radiolabel purified proteins using the Iodogen method, with modified tyrosine residues on the surface of proteins, as described (Fraker & Speck, 1978). 150 µg of all recombinant proteins were separately ^{125}I -labelled and dialyzed exhaustively against phosphate-buffered saline overnight at 4°C to remove non-protein-bound radioactivity. Subsequently, CD-1 mice (n=6) were injected with 10 million cpm rEcall-modified proteins of comparable specific activity (~1 x 10^7 cpm/mg), and serial blood samples were taken from the tail over the course of 24h until residual radioactivity fell below 1% initial values. Next, acid-precipitated plasma samples were analyzed by γ-counting (Packard Cobra II counter) to measure protein-bound plasma radioactivity. Thereafter, data was normalized, with the plasma protein-bound radioactivity contained in the 2-minute post-injection blood sample being defined as 100%. Area under the observed clearance curve (AUC) was identified using GraphPad Prism 9.

It is important to note that for first clearance experiment (examining H_6-rEcall, H_6-rEcall-ABD, H_6-rEcall-HSA), 150 ug of proteins were mixed with I-125 (1mCi) for 5 minutes. Whereas, in the second clearance experiment (observing rEcall-H_6, HSA-rEcall-H_6, H_6-rEcall-HSA, and HSA-rEcall-H_6), the reaction time was shorter; 150 ug of proteins were mixed with I-125 for 1 minute.

2.16 RAP and GST Transformation

Receptor-associated protein (RAP) was obtained as a Glutathione sulfotransferase (GST) fusion protein (GST-RAP) as previously described (Sheffield et. al, 2018). Purified plasmid DNA of pGEX-GST-RAP and pGEX-GST were transformed into E. coli BL21 cells, performed as aforementioned.

2.17 Expression in *E. coli* and Purification

Mid-log phase cultures of E. coli BL21 transformed with pGEX-GST (500 ml) or pGEX-RAP (3.0 L) were induced by the addition of 0.1 mM isopropyl ß-D-1-thiogalactopyranoside (IPTG) to the culture medium, as described (Bhakta, 2021). After 4 hours of induction at 225rpm and 37^{o}C, cells were harvested by centrifugation (Sorvall LYNX 6000 superspeed centrifuge, Thermo Fisher Scientific) at 6,000 rpm at 4^{o}C for 30 mins, resuspended in PBS with protease inhibitors (Complete, Roche), and lysed by sonication. Sonication took place for 3 minutes at an amplitude of 30% with 5 seconds on and 5 seconds off pulses (Sonics Vibra Cell Sonicator model VCX500). Thereafter, pGEX-GST lysate was adjusted to 1% (vol/vol) Triton X-100 and incubated with 2 mL of (20% slurry) glutathione agarose beads. Protein suspension was transferred to columns, washed with PBS, and purified using affinity chromatography on glutathione-Sepharose as previously described (Bhakta, 2021).

2.18 Concentrating pGEX-RAP & pGEX-GST

Eluted fractions were pooled, dialyzed, concentrated, and their protein concentrations were determined using Bradford assays, as above.

2.19 Injecting IVIg, pGEX-RAP, and pGEX-GST in CD-1 mice

1mL (150 µM) of GST-RAP or GST were mixed with ^{125}I-labelled H_6-rEcall-HSA and injected via the tail vein. 2.5 g/kg Intravenous immunoglobulin (IVIg) was administered intraperitoneally 24 hours before ^{125}I-labelled H_6-rEcall-HSA.

2.20 Organ Distribution

By intraperitoneally injecting 2.5% (w/vol) of tribromoethanol (Sigma-Aldrich), mice were anesthetized in order to cannulate the right jugular vein and deliver (~1 x 10^7 cpm) ^{125}I-rEcall-H_6 or ^{125}I-HSA-rEcall-H_6. After 30 minutes, mice were sacrificed, and four organs were excised and rinsed in ice-cold saline. The four organs were the liver, kidneys, spleen, and heart. Using a Packard Cobra II counter, a γ-counter, organ-associated radioactivity was then measured.

2.21 Mass Spectrometry

H_6-rEcall molecular mass was confirmed by liquid chromatography mass spectrometry (LCMS) using positive ion electrospray ionization (ESI) in the McMaster Regional Centre for Mass Spectrometry. Data were acquired on an Agilent 1290 Infinity II UPLC coupled to an Agilent 6550 Q-ToF. The column used was a Jupiter C4 column 5 µm particle size, 4.6 mm x 250 mm, 300Å manufactured by Phenomenex. 5 µl of 0.5 µg/ml H_6-rEcall was injected onto the column. Unfused rEcall eluted at 3.9 minutes. The extracted spectrum showed multiply charged peaks corresponding to $[M+5H]^{5+}$ at m/z 1508, $[M+6H]^{6+}$ at m/z 1257, etc. Deconvolution of the spectrum was performed using Agilent Bioconfirm software.

2.21 Statistical analyses

Data were analyzed using GraphPad Prism 9. A p-value of < 0.05 was taken to indicate statistical significance. For multiple comparisons, data were assessed using one-way ANOVA; * *p<0.05, ** p<0.01, *** p<0.001, **** p<0.0001,* and results are reported as means ± one standard deviation (SD) (n=5-6).

3.0 Results

3.1 Restriction Endonuclease Digestion

It was necessary to examine DNA fragments by agarose gel electrophoresis at multiple points during this study. An example of one such analysis is shown in Figure 6. To confirm that DNA was digested correctly following incubation with XhoI and EcoRI, H_6-rEcall and pZAMP plasmid DNA was electrophoresed on an agarose gel. Single bands of 228 bp and 4554 were observed, as expected (see Table 1).

Figure 6: DNA electrophoresis. 1.1% agarose gels stained with ethidium bromide are shown, with the plasmids whose XhoI-EcoRI-digested DNA fragments were electrophoresed identified above the lanes. Markers (to the left) are 1kb+ (Invitrogen); the positions of the 5000 and 200 bp marker are identified by labels.

3.2 Ligation and Transformation:

It was also necessary to verify that clones of E. coli transformed with ligated reaction mixtures had the predicted restriction endonuclease pattern, as an initial diagnostic step carried out prior to selecting clones for verification by DNA sequencing. An example of such clonal screening is shown in Figure 7. Three clones which were candidates for pZAMP-H_6-rEcall were restricted with HindIII. All showed a single band after restriction, in contrast to pZAMP vector, which yielded two fragments.

Figure 7: DNA gel electrophoresis. A 1.1% agarose gel stained with ethidium bromide presenting pZamp and H_6-rEcall plasmids restricted with HindIII to differentiate between the vector and recombinant proteins, is shown. The first well to the left is the 1 kb+ DNA ladder, the second well is pZAMP, and the following wells are three H_6-rEcall clones, following HindIII digestion.

3.3 Protein Expression and Purification

Recombinant proteins encoded by the engineered expression plasmids were expressed in *P. pastoris* X33 and purified from conditioned media, or, in the case of GST and GST-RAP, in *E. coli* BL21 and purified from clarified cell lysates. H_6-tagged proteins were purified by nickel chelate affinity chromatography, while GST-tagged proteins were purified via glutathione affinity chromatography. Figure 8A shows that H_6-rEcall-ABD (14 kDa), and rEcall-H_6 and H_6-rEcall (12 kDa) were purified to apparent homogeneity, judging by the single polypeptide bands found in these preparations. H_6-rEcall-HSA comprised a major polypeptide band of 75 kDa, an

expected molecular weight greater than the 67 kDa Bovine Serum Albumin (BSA) marker, and a minor polypeptide band of approximately 54 kDa. Figure 8B displays that HSA-rEcall-H_6 comprised a single polypeptide band of expected molecular weight 75 kDa, greater than BSA. The N- or C- terminally HSA-tagged rEcall proteins, like KPI-HSA (Sheffield et al, 2018), reacted with anti-hexahistidine antibodies on immunoblots (Figure 9). Furthermore, Figure 10 shows that GST (27 kDa) was purified to apparent homogeneity, while GST-RAP preparations comprised a single major polypeptide of 65 kDa and some less abundant smaller molecular weight species.

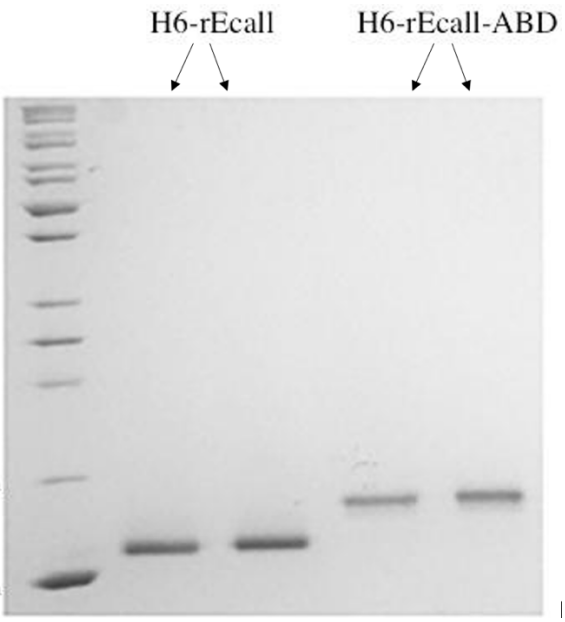

Figure 8: Protein gel electrophoresis of N and C-terminally H_6-tagged rEcall proteins. SDS polyacrylamide gels electrophoresed under reducing conditions and stained with Coomassie Brilliant Blue are shown (A, 15% w/vol ; B, 10% w/vol). Purified proteins are identified above the lanes. BenchMark Protein ladder with selected markers (70, 60, and 50 kDa) is shown at left.

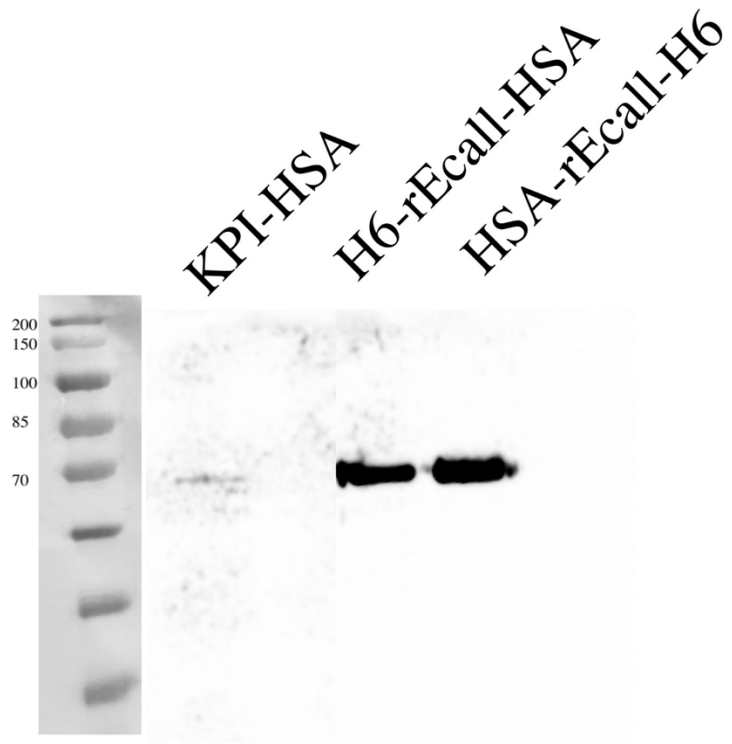

Figure 9: Western blots displaying N- or C-terminally HSA-tagged rEcall proteins. They were immunoblotted with anti-hexahistidine antibodies. Proteins are described above the lanes. KPI-HSA was used as a positive control. Marker and sizes in kDa are at left.

Figure 10: Protein gel electrophoresis of GST-containing proteins. As in Figure 4, a Coomassie-stained 10% SDS-polyacrylamide gel is presented, with purified proteins identified above the lanes and ladder at left.

Table 2 shows representative concentrations and overall yields of protein purifications of all recombinant proteins used in this study. Bradford assay results in general were supported by electrophoresing 1 µg of the presumed protein concentrations on SDS PAGE and comparing them to the same weight of a BSA standard.

Table 2: Protein concentrations and yields determined by Bradford assays.

Type of Recombinant Protein	Concentration (mg/ml of purified solution)	Protein yield (mg)	Yield (mg/L of culture volume)
H_6-rEcall	1.7	0.84	0.84/ 3= 0.30
H_6-rEcall-ABD	4.1	2.1	2.1/3 = 0.70
H_6-rEcall-HSA	3.0	1.5	1.5/3= 0.50
rEcall-H_6	2.0	1.0	1/3= 0.33
HSA-rEcall-H_6	2.8	1.4	1.4/3= 0.50
HSA- H_6	9.3	4.7	4.7/1= 4.7
pGEX-GST	22	11.5	11.5/0.5= 23
pGEX-RAP	10	4.5	4.5/3= 1.5

3.4 Kinetic characterization of rEcall proteins as inhibitors of PK

Inhibitory constants (K_i) were determined for each rEcall protein by determining the velocity of PK-mediated S2302 amidolysis at different substrate concentrations, in the presence of varying concentrations of rEcall proteins acting as inhibitors. Michaelis-Menten curves are shown in Figure 11 and their reciprocal transformations, also called Lineweaver-Burke graphs, as shown in Figure 12 and 13.

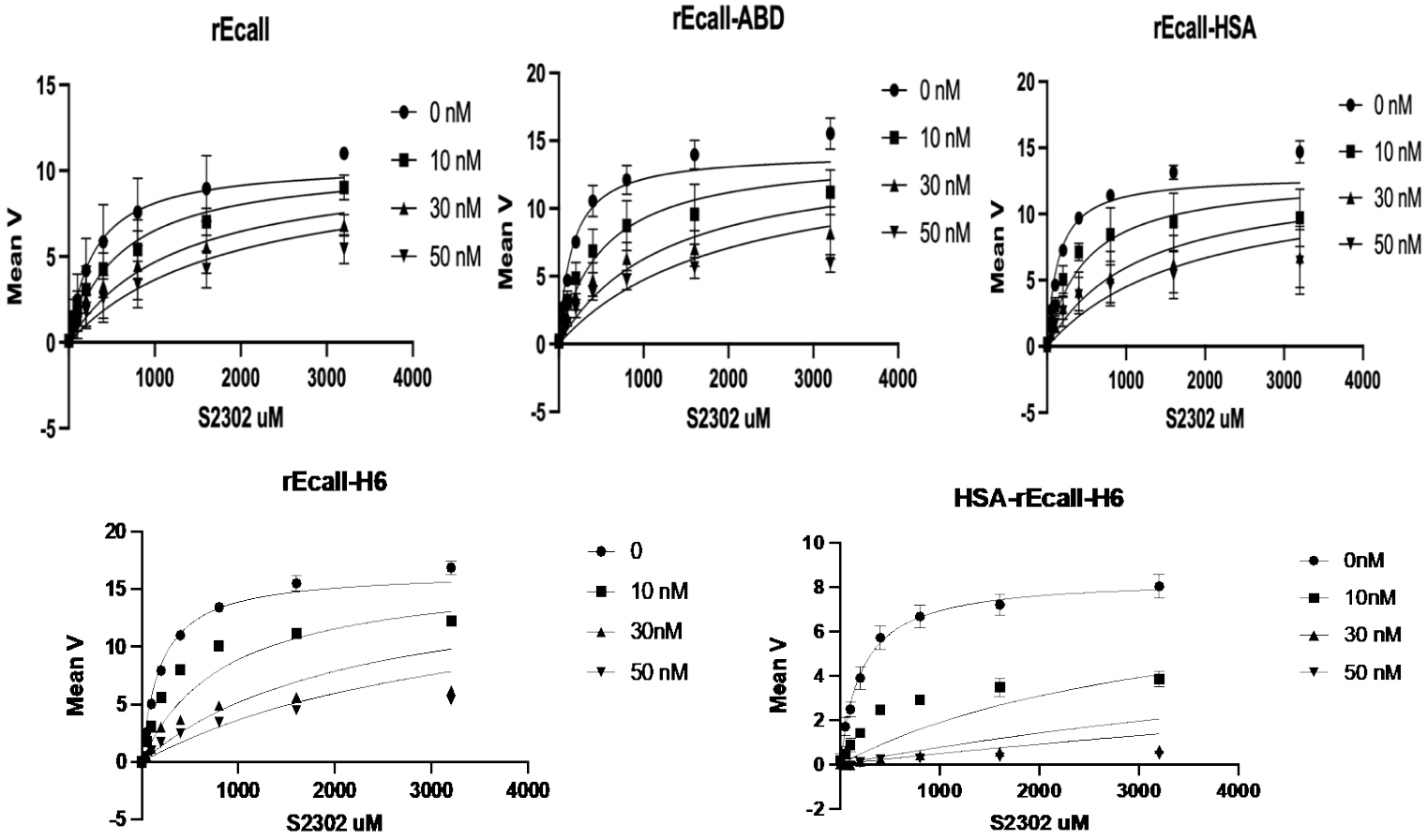

Figure 11: Michaelis-Menten analysis of initial rEcall proteins. Graphs illustrate the competitive inhibition of PK by all rEcall proteins; specified on top of each graph. Each point is the mean of 5 determinations ± SD. Y-axis represents the rate of substrate (S2302) cleavage by PK, whereas the x-axis is substrate concentrations. Recombinant protein concentrations are depicted at right. Data points are arithmetic means ± SD (n= 5), with downward pointing error bars (invisible in some cases due to their small size).

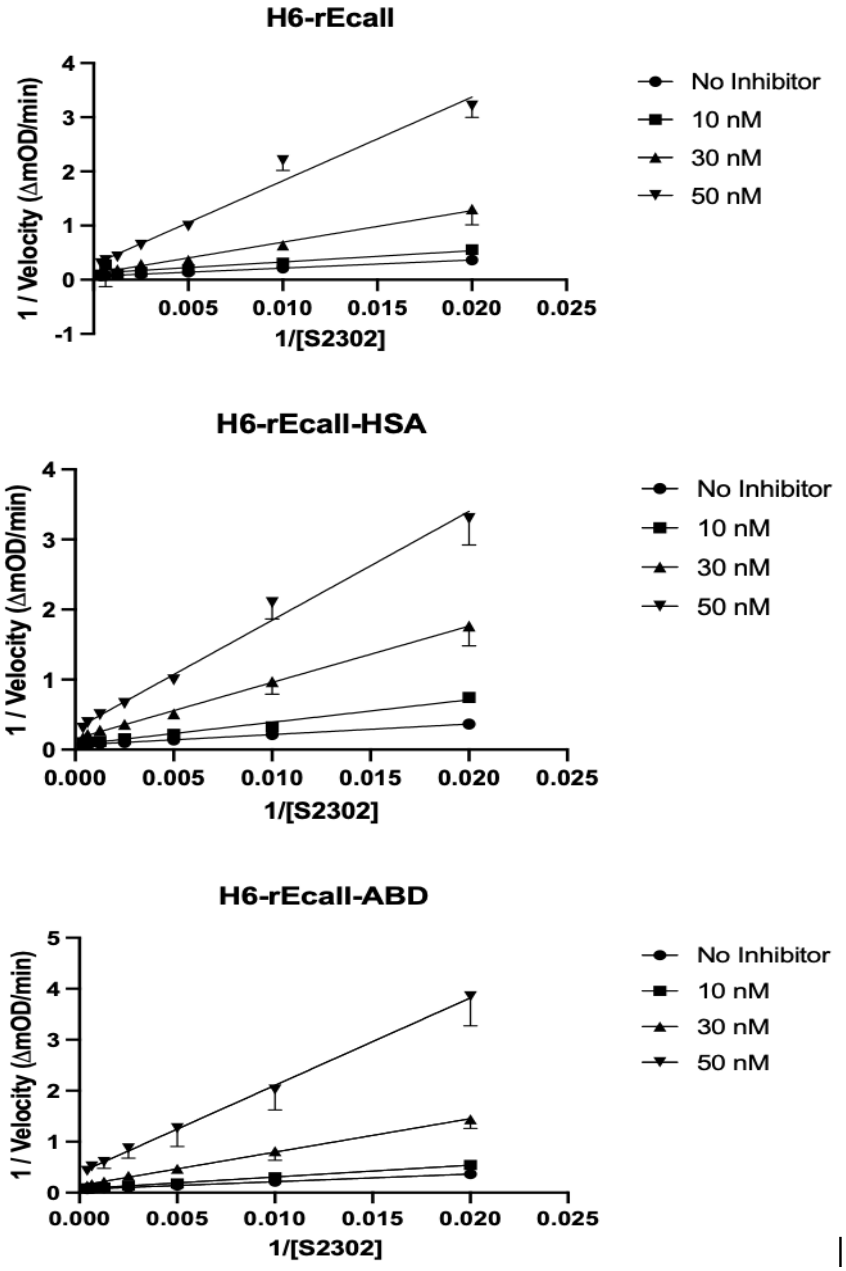

Figure 12: Lineweaver-Burke plots. Graphs show the reciprocal of reaction velocity vs. the reciprocal of S2302 concentration. Inhibitor proteins are indicated above each graph, and correspond to H_6-rEcall, H_6-rEcall-ABD, H_6-rEcall-HSA, and HSA-rEcall-H_6 (n=5 ± SD). The different protein concentrations are indicated on the top right of each plot. Plots were used to derive the K_i values of each protein. Data points are arithmetic means ± SD (n= 5), with downward pointing error bars (invisible in some cases due to their small size).

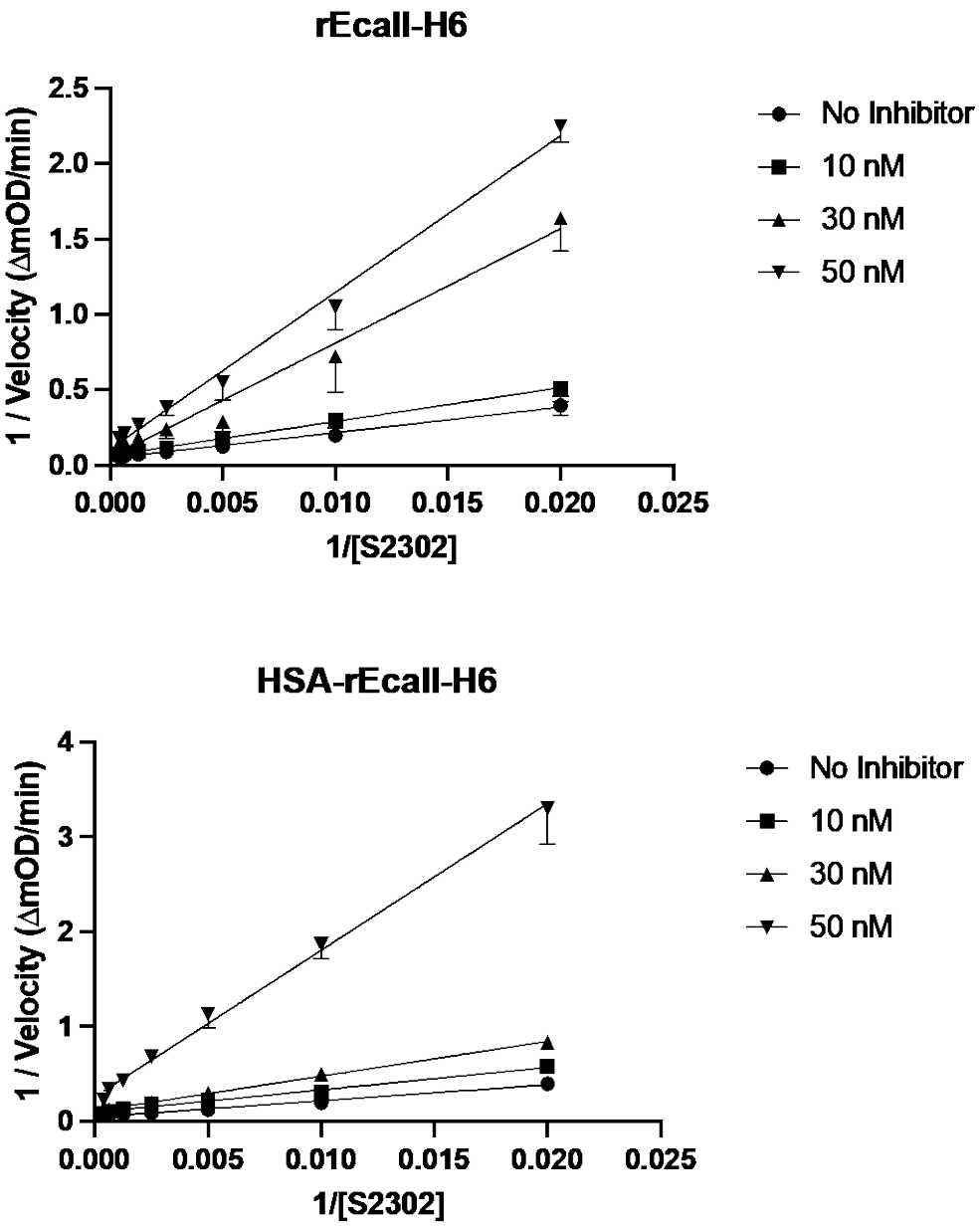

Figure 13: Lineweaver-Burke plots. Graphs display the reciprocal of reaction velocity vs. the reciprocal of S2302 concentration. Inhibitor proteins are denoted above each graph and correspond to HSA-rEcall-H_6 and rEcall-H_6 (n=5 ± SD). As in Figure 12, protein concentrations are specified at right. Plots were used to derive the K_i values of each protein.

Figure 14 presents the results of replicated measurement of K_i values. Mean values were largely unaffected by the position of the hexahistidine tag or the relative orientation of the rEcall and HSA domains of the fusion proteins. Mean K_i values ranged from 2.22 ± 0.12 nM for H_6-rEcall-HSA to 2.91 ± 0.42 nM for H_6-rEcall. Within this narrow range, K_i values did not differ statistically among H_6-rEcall, H_6-rEcall-ABD, rEcall-H_6, or HSA-rEcall-H_6. H_6-rEcall-HSA had a significantly lower mean K_i value, and thus greater inhibitory potency, than any other protein.

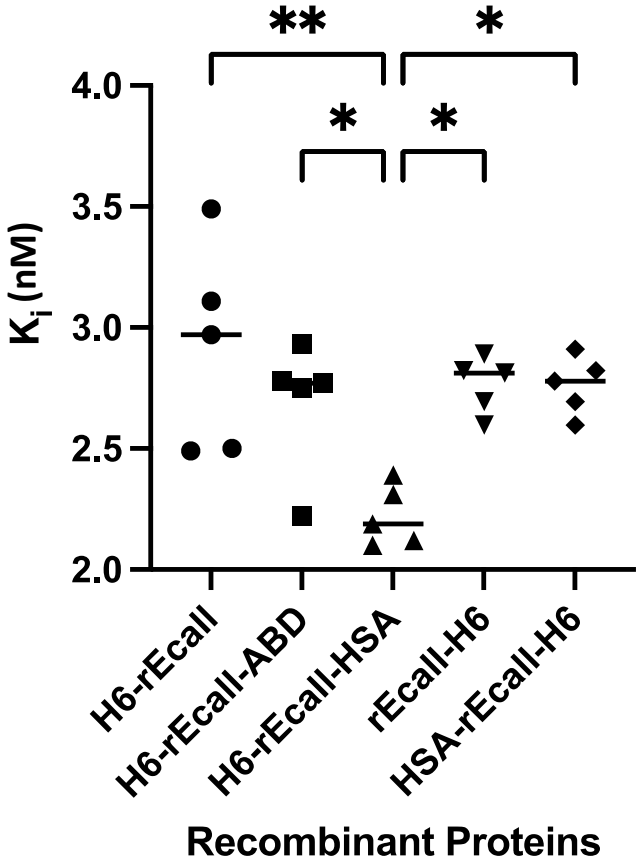

Figure 14: Graphical comparison of K_i values. Each point represents an independent K_i determination for proteins listed on the x-axis (n=5). Horizontal lines show the mean. *, $p < 0.01$; **, $p < 0.05$.

Table 3: K_i values obtained from conducting chromogenic assays. 1nM PK, 0-3200 µM S2302, and 0-50 nM recombinant proteins.

Proteins	**Trial 1 K_i (nM)**	**Trial 2 K_i (nM)**	**Trial 3 K_i (nM)**	**Trial 4 K_i (nM)**	**Trial 5 K_i (nM)**	**Mean (nM)**	**SD**
H_6-rEcall	2.50	2.49	3.11	2.97	3.49	2.91	0.42
H_6-rEcall-ABD	2.22	2.75	2.78	2.77	2.93	2.69	0.27
H_6-rEcall-HSA	2.12	2.31	2.19	2.10	2.39	2.22	0.12
rEcall- H_6	2.60	2.82	2.70	2.78	2.91	2.76	0.12
HSA-rEcall- H_6	2.58	2.51	2.95	2.52	2.92	2.69	0.22

3.5 Gel-based analysis of inhibition of macromolecular reactions catalyzed by PK

To test whether the similar inhibitory potency of all rEcall proteins observed for the inhibition of PK-catalyzed cleavage of a small chromogenic substrate extended to the macromolecular targets of PK, gel-based analyses were conducted. PK-catalyzed cleavage of high molecular weight Kininogen (HK), factor XII (FXII), and factor IX (FIX, with calcium ions) were examined. PK cleaved HK (120 kDa) producing a heavy and light with sizes of 62 and 48 kDa, respectively (Dobó et. al, 2011). FXII has a size of 80 kDa, and when cleaved it produces a heavy and light chain around the 80 and 30 kDa mark (Cugno et. al, 2014). Finally, FIX has a size of 57 kDa and generates a heavy chain of 30 kDa and a light chain of 20 kDa (Samis et. al, 2000). Recombinant proteins comparably fully/partially hindered PK from cleaving all its proteases; HK, FXII, and FIX. This is evident by the absence of bands around 62 and 48 kDa for the cleavage of HK, 80 and 30 kDa for FXII, and 30 and 20 kDa for FIX, in the presence of any of the three rEcall proteins tested (Figure 15-17).

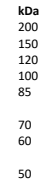

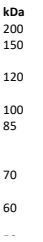

Figure 15: Gel-based analysis of PK-mediated cleavage of HK. Coomassie-stained 10% SDS polyacrylamide gels electrophoresed under reducing conditions are shown. The absence of a component is illustrated by "-" and the presence by "+". Molecular weight markers are as presented in Figure 8. A) PAGE resembling full inactivation of HK cleavage by rEcall proteins. B) Partial HK cleavage by PK. Reactions illustrating full inhibition were incubated for 1h-2h at 37 °C, whereas reactions demonstrating partial cleavage were incubated for 15- 40 mins.

Figure 16: Gel-based analysis of PK-mediated cleavage of FXII. Coomassie-stained 10% SDS polyacrylamide gels electrophoresed under reducing conditions are shown. As in Figure 15, reaction components are displayed below each panel and ladder is at left. C) Full inhibition of FXII cleavage by rEcall proteins. D) Partial FXII cleavage by PK. As aforementioned, reactions were incubated for 1h-2h and 15- 40 mins at 37 °C, respectively.

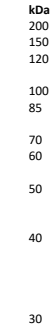

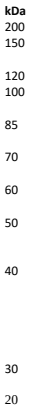

Figure 17: Gel-based analysis of PK-mediated cleavage of FIX. Coomassie-stained 10% SDS polyacrylamide gels electrophoresed under reducing conditions are shown. Reaction components are depicted below each panel and markers are at left. E) Full inactivation of FIX cleavage by recombinant proteins. F) Partial FIX cleavage by PK in the presence of Ca+. Reactions included H_6-rEcall, H_6-rEcall-ABD, or H_6-rEcall-HSA. At 37 °C, reactions were incubated for 1h-2h or 15- 40 mins.

3.6 Reaction of rEcall proteins with different serine proteases

To test whether rEcall proteins were specific for PK or were able to inhibit other proteases, rEcall proteins were introduced into chromogenic substrate reactions with different proteases. As shown in Figure 18A, PK exhibited the most substantial rEcall-mediated inactivation. Inhibition of FXIa and plasmin (PLSN) was also detected (Figs 18B and C). The same profile was observed for H_6-rEcall and H_6-HSA-rEcall (Fig 19). In contrast, no substantial inhibition of thrombin, FXIa, or FXa was observed involving both fused and unfused rEcall proteins.

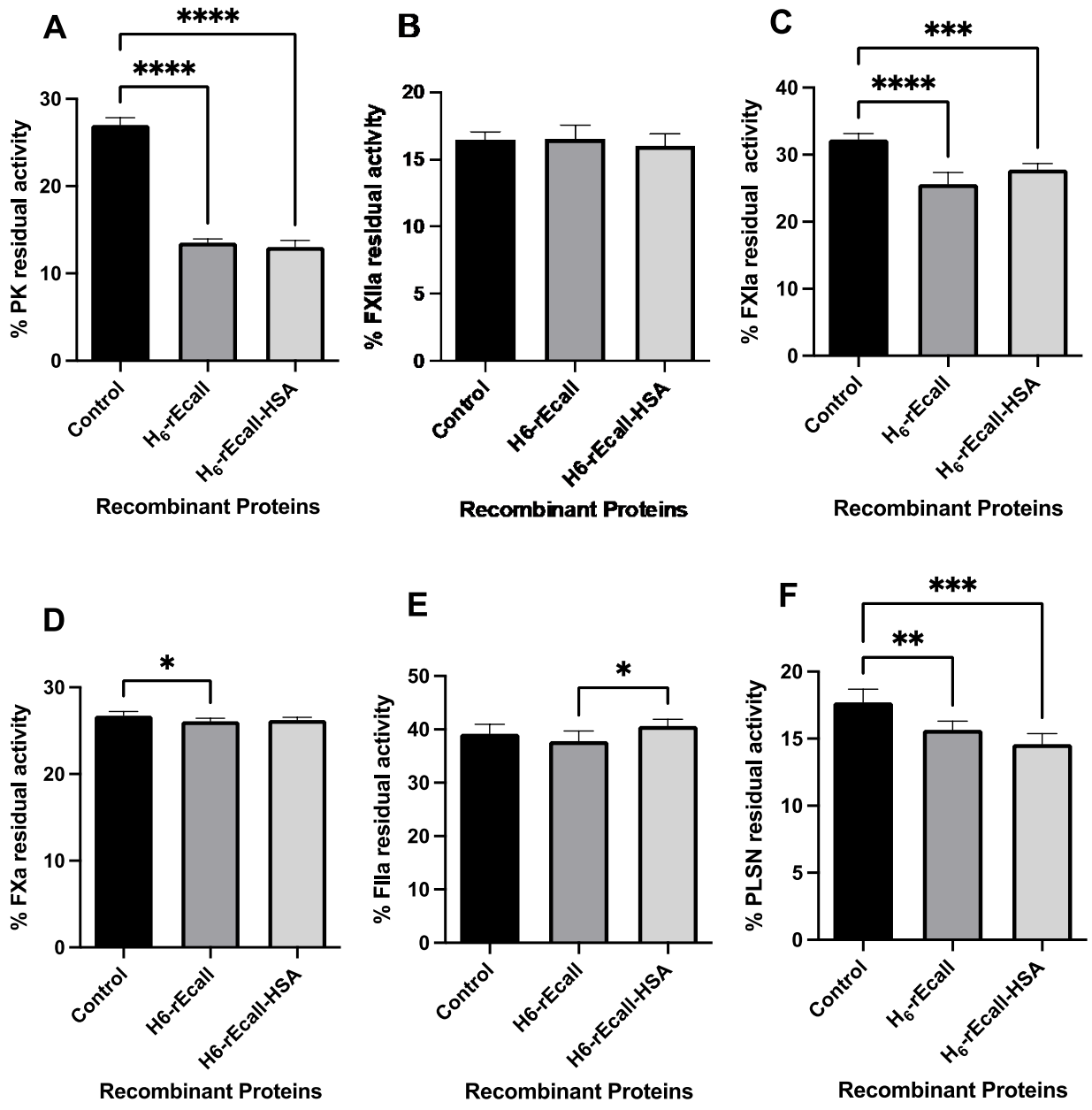

Figure 18: Comparison of effects of rEcall proteins on several serine proteases. Activities of different proteases on their corresponding chromogenic substrates were measured in the absence (PPNE buffer alone) or presence of rEcall proteins identified on the x-axis. Proteins (PK, FXIa, PLSN, FIIa, FXIIa, and FXa, are identified on the y-axis. The mean of 5 determinations ± SD is shown. Statistical comparisons between groups identified by horizontal brackets are indicated by * $p<0.05$, ** $p<0.01$, *** $p<0.001$, **** $p<0.0001$.

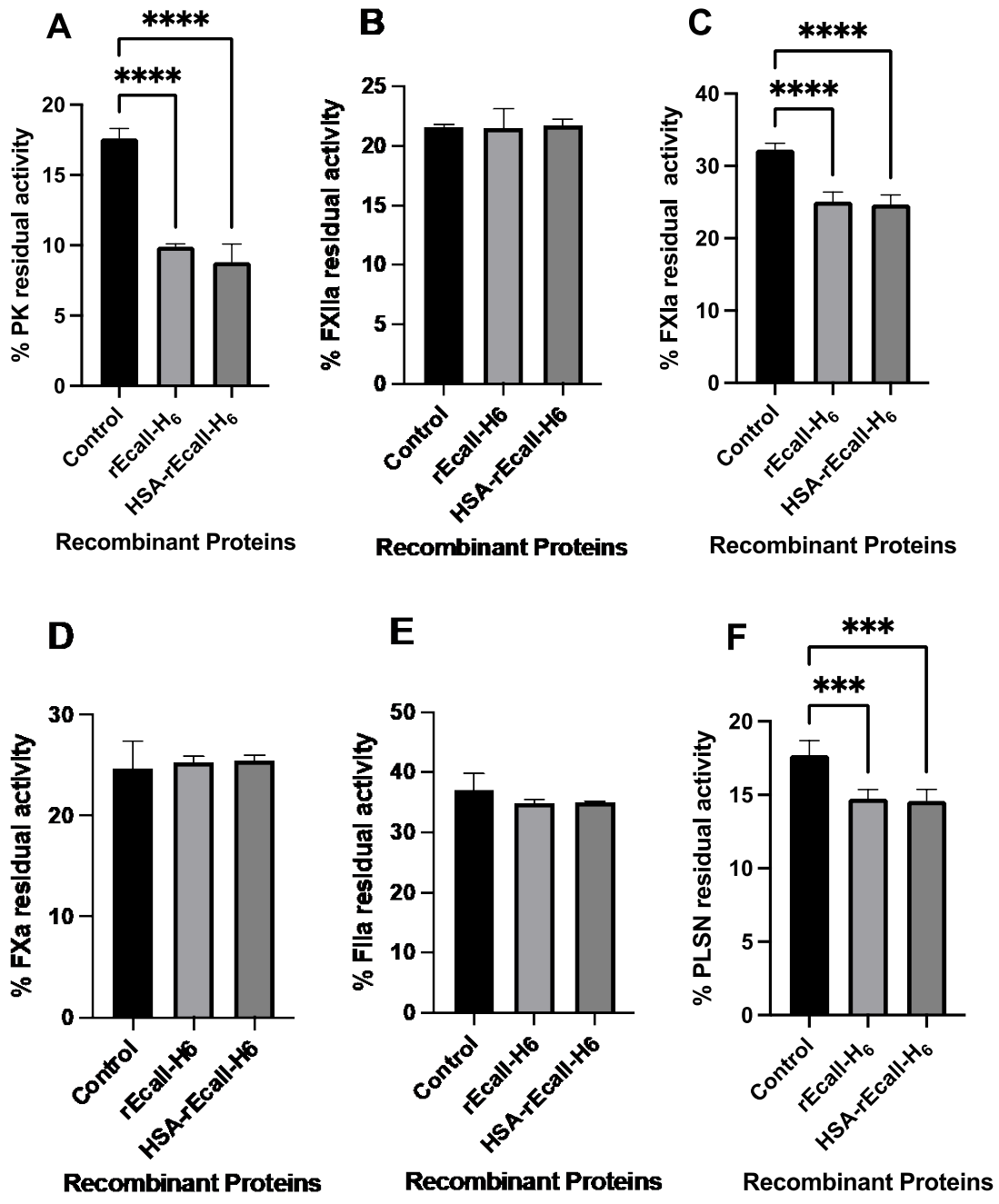

Figure 19: Comparison of effects of rEcall proteins on various serine proteases. As in Figure 18, the interaction between proteases and their respective chromogenic substrates was monitored in the absence or presence of rEcall proteins (n=5, mean± SD). Y-axis represents the proteases and x-axis represents C-terminally H_6-tagged rEcall proteins. Statistical comparisons between groups identified by horizontal brackets are indicated by *** $p<0.001$, **** $p<0.0001$.

3.7 In vivo clearance of rEcall proteins in mice

In vivo clearance of rEcall proteins was followed by radiolabeling the proteins with ^{125}I, injecting the radiolabeled proteins into the circulation of mice intravenously, and following acid-precipitable radioactivity remaining in plasma samples over time. It was not practical to label and test all proteins at the same time. Accordingly, three proteins were examined first: H_6-rEcall; H_6-rEcall-ABD; and H_6-rEcall-HSA. As shown in Figure 20, H_6-rEcall-HSA remained in the murine circulation longer than the other two forms of rEcall. Quantitatively, 2 hours post-injection, 26 ± 2 % of H_6-rEcall-HSA remained in circulation vs. 7 ± 1% of H_6-rEcall-ABD and 6 ± 2 % of H_6-rEcall ($p < 0.0001$). In these experiments, baseline 100% levels were set as the amount of radioactivity associated with each protein in plasma samples taken two minutes post-injection.

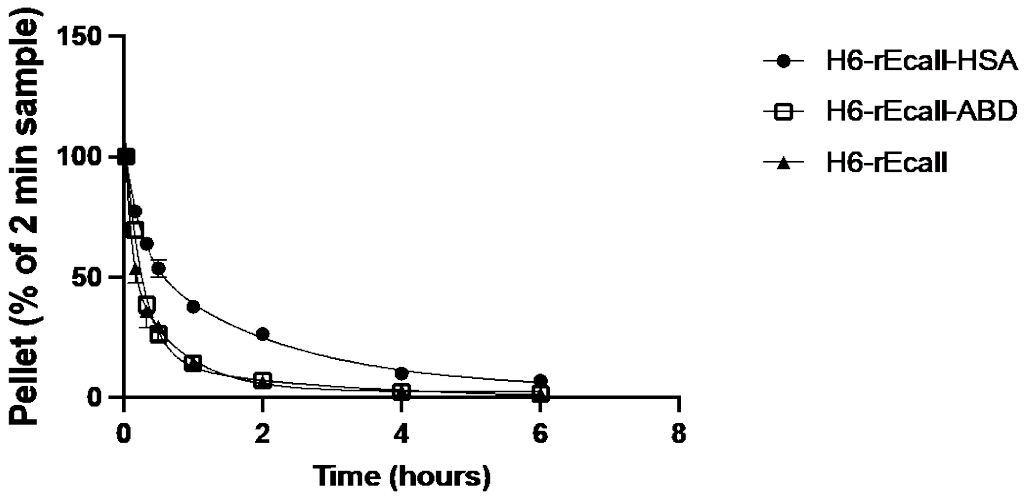

Figure 20: In vivo clearance of N-terminally H_6-tagged rEcall proteins in mice. % Residual radioactivity of ^{125}I-labelled proteins after intravenous injection in mice vs. time post-injection (n=6 ± SD). Proteins radiolabelled and injected were H_6-rEcall, H_6-rEcall-ABD, and H_6-rEcall-HSA, as illustrated on the top right. Data points were normalized to the radioactivity present in the initial 2-minute plasma sample from each mouse. Data points are arithmetic means ± SD (n= 6), with downward pointing error bars (invisible in some cases due to their small size.

Subsequently, the analysis was expanded to include HSA-H_6, as a control protein previously demonstrated to clear slowly in mice, and HSA-rEcall-H_6. The data were plotted and normalized to the plasma radioactivity two minutes after injection. Figure 21 shows that HSA-H_6 remained in the circulation to a much greater extent than any of the rEcall proteins since much greater amounts of HSA-H_6-associated radioactivity remained in the circulation at all time points. The order of proteins remaining in the circulation was HSA- H_6> H_6-rEcall-HSA ≥ HSA-rEcall- H_6> rEcall-H_6. More quantitatively, 2 hours post-injection, 50 ± 10 % of H_6-rEcall-HSA was recovered in the circulation vs. 12 ± 3 % of rEcall-H_6 ($p < 0.0001$). Additionally, 36 ± 6 % of HSA-rEcall-H_6 remained vs. 75 ± 5 % of HSA- H_6 ($p < 0.0001$).

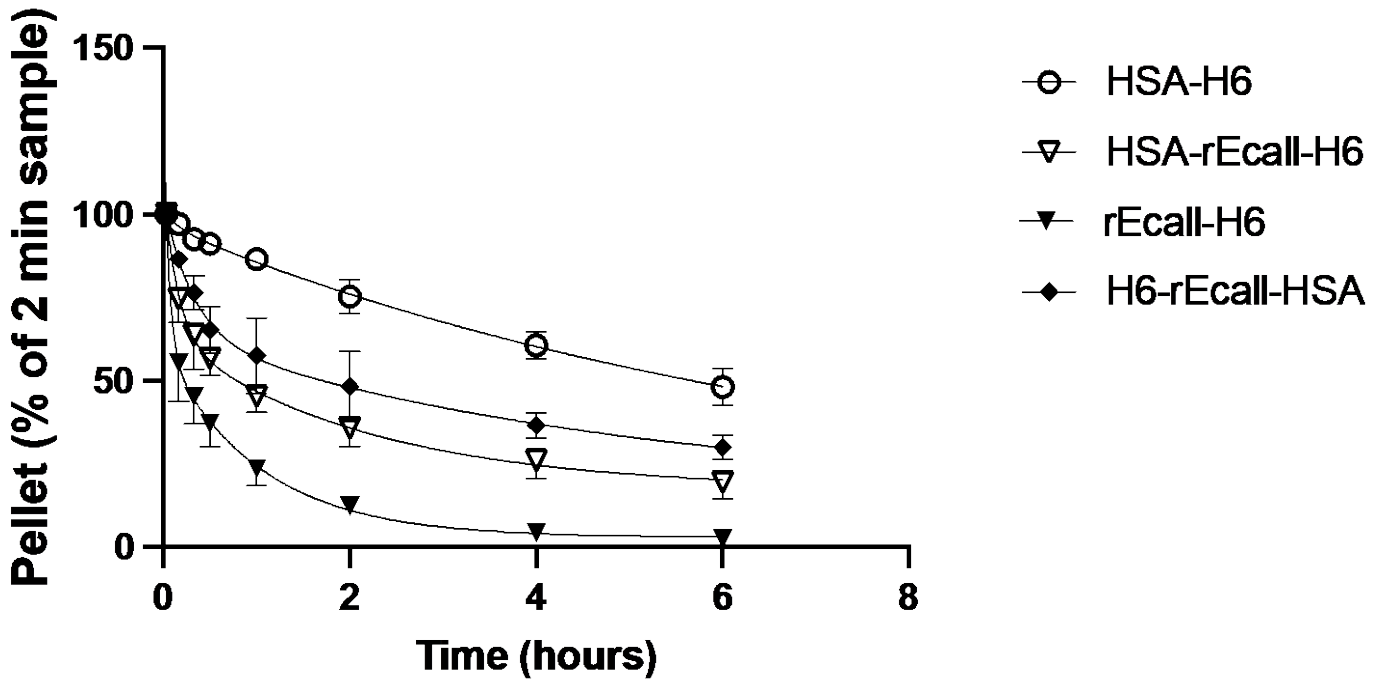

Figure 21: In vivo clearance of rEcall proteins in mice. % Residual radioactivity of ^{125}I-labelled proteins after intravenous injection in mice vs. time post-injection (n=6, mean ± SD). Proteins radiolabelled and injected were rEcall-H_6, H_6-rEcall-HSA, HSA-H_6, and HSA-rEcall-H_6. Plots show proteins remaining in mice across the span of 24 hours. As in Figure 18, data points were normalized to the radioactivity present in the initial 2-minute sample of the mouse.

Figure 22 displays the percentage of normalized protein-associated radioactivity remaining in the circulation after 30 minutes of injection for the experiments shown in Figure 21. As presented, 65.3 ± 6.9 % of H_6-rEcall-HSA was recovered in the circulation vs. 37.1 ± 7% of rEcall-H_6 ($p < 0.0001$). Additionally, 56.8 ± 5.2 % of HSA-rEcall-H_6 remained vs. 91.2 ± 1.6% of HSA- H_6 ($p < 0.0001$).

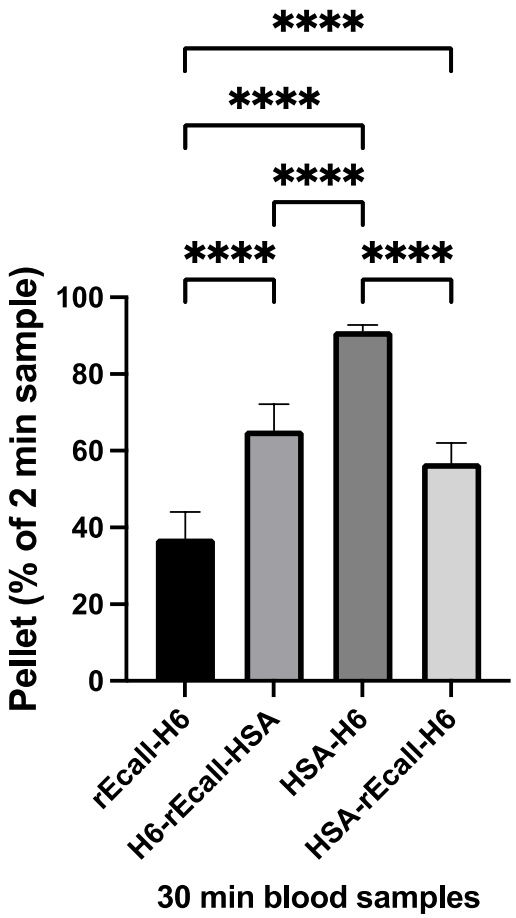

Figure 22: % Radiolabeled protein recovery 30 mins after injection. ^{125}I-labelled proteins observed were rEcall-H_6, H_6-rEcall-HSA, HSA-H_6, and HSA-rEcall-H_6 (identified on the x-axis). The y-axis represents the % protein recovered of the total amount injected after 30 mins. As in Figure 18, data points were normalized to the radioactivity present in the initial 2-minute sample of the mouse. Statistical comparisons between groups identified by horizontal brackets are indicated by * $p<0.05$, ** $p<0.01$, *** $p<0.001$, **** $p<0.0001$.

3.8 Competition Experiment

To gain information regarding which receptors may be involved in rEcall protein elimination from the murine circulation, competition experiments were performed. Briefly, GST-RAP was used as a competitor of clearance via the Lipoprotein receptor Related-Protein 1 (LRP1) receptor (He et al., 2021). Purified human Immunoglobulin G (IVIg) was used as a competitor of the neonatal Fc receptor (FcRn) (Sleep, 2013). Doses of these competitors previously shown to compete with these receptor-mediated clearance pathways were co-administered (GST and GST-RAP) or administered intraperitoneally the night before (IVIg) due to injection volume constraints (Sheffield et al., 2018). ^{125}I-H$_6$-rEcall-HSA was selected as the protein for competition to gain insights as to why rEcall clearance was not more like HSA clearance after HSA fusion.

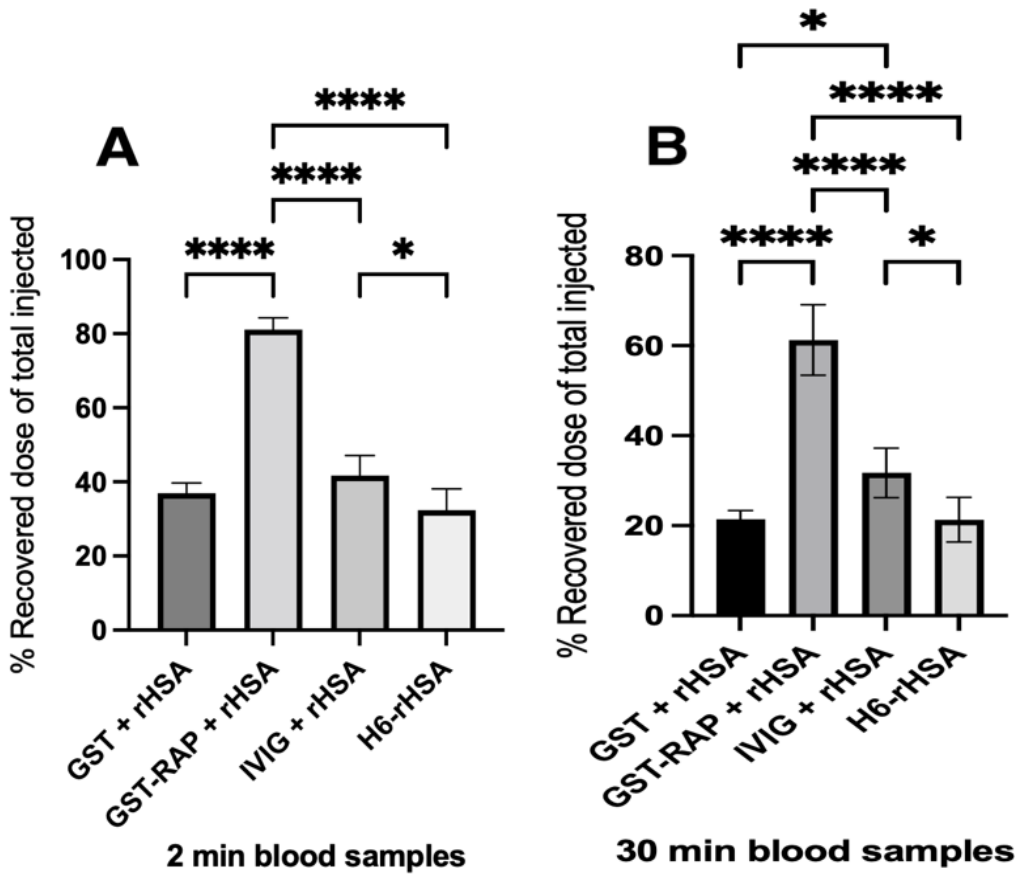

Figure 23: In vivo clearance competition experiments. % ^{125}I- H_6-rEcall-HSA circulation in presence of GST, GST-RAP, or IVIg. Samples were obtained 2 and 30-mins post-injection (n=5 ± SD). As in Figure 20, the y-axis represents the % protein of total amount injected A) after 2 mins and B) after 30 mins. Treatments are indicated below the x-axis. Statistical comparisons between groups identified by horizontal brackets are indicated by * $p<0.05$ and **** $p<0.0001$.

Figure 23 shows that competition with GST had no effect on rEcall-HSA recovery after 2 and 30 minutes of injection, as it did not differ statistically from rEcall-HSA recovery with no competitor. In contrast, GST-RAP competition elevated the recovery of ^{125}I- H_6-rEcall-HSA 2.2-fold, from 37 ± 3 % for GST + H_6-rEcall-HSA to 81 ± 3 % for GST-RAP + H_6-rEcall-HSA. Competition with IVIg also significantly increased the recovery of ^{125}I- H_6-rEcall-HSA, but to a lesser degree, by 1.13-fold (to 42 ± 5% for IVIg + H_6-rEcall-HSA). Similar significant changes were also observed 30 mins after injection, of 2.9- and 1.9-fold, respectively.

3.9 Analyzing Clearance Profiles

Another way of quantifying residency time of a protein in the plasma compartment is to measure the observed Area Under the clearance Curve (AUC). AUC values corresponding to the clearance curves shown in Figure 21 are shown in Table 4. The results show that fusing the ABD domain to H_6-rEcall did not alter its plasma residency profile but that fusing HSA to H_6-rEcall slowed its clearance, as evidenced by the statistically significant 3.3-fold increase in mean AUC for H_6-rEcall-HSA. Similarly, Table 5 shows that both H_6-rEcall-HSA and HSA-rEcall-H_6 fusion proteins remained in the mouse circulation longer than unfused rEcall- H_6, by factors or 5.3-fold and 3.8-fold, respectively. Although the plasma residency of both fusion proteins was extended relative to either H_6-rEcall or rEcall-H_6, neither fusion protein remained in the moue circulation as long as HSA-H_6, which persisted in the plasma 8.5-fold longer, on average, than rEcall-H_6.

Table 4. Area under the Clearance Curve (AUC) profiles of H_6-rEcall, H_6-rEcall-ABD, and H_6-rEcall-HSA in mice. The AUC of clearance curves shown in Figure 20 is shown. Data are mean values ± SD, n=6; **** $p < 0.0001$ vs. H_6-rEcall (ANOVA).

Proteins	AUC (% hours)
H_6-rEcall	77± 10
H_6-rEcall-ABD	75 ± 9
H_6-rEcall-HSA	250 ± 10****

Table 5. Area under the Clearance Curve (AUC) profiles of rEcall-H_6, H_6-rEcall-HSA, HSA-rEcall-H_6, and HSA-H_6 in mice. The AUC of clearance curves shown in Figure 21 is shown. Data are mean values ± SD, n=6; **** $p < 0.0001$ vs. rEcall-H_6 (ANOVA).

Proteins	AUC (% hours)
rEcall-H_6	120 ± 20
H_6-rEcall-HSA	620 ± 50****
HSA-rEcall-H_6	440± 80****
HSA-H_6	980± 40****

3.10 Organ distribution

Fusion to albumin changed rEcall-H_6's organ distribution (Figure 24). Of the four organs extracted 30 minutes after injection, rEcall-H_6 was predominantly found in the kidneys, and fusion to albumin largely redirected rEcall to the liver. 3.6-fold more HSA-rEcall-H_6 was found in the liver in comparison to rEcall-H_6 ($p<0.0001$). In contrast, 3.3-fold more rEcall-H_6 was observed in the kidneys vs. HSA-rEcall-H_6 ($p<0.0001$).

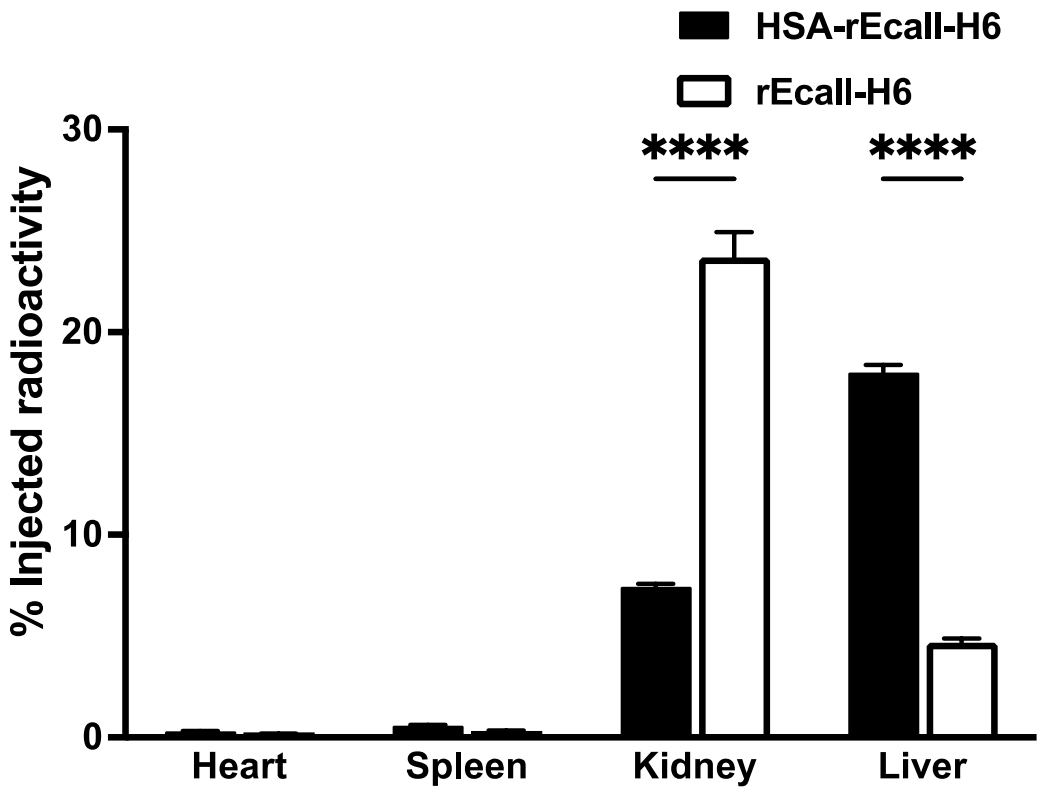

Figure 24: **The percentage of the total ^{125}I-labelled rEcall-H_6 or ^{125}I -HSA-rEcall-H_6 recovered 30 minutes post-injection.** For rEcall (white bars) and rEcall-HSA (black bars) are shown for each of four organs identified on the x-axis (means ± SD, n=5). Four organ samples were extracted from each mouse. Statistical comparisons between groups identified by horizontal brackets are indicated by **** $p<0.0001$.

3.11 Mass Spectrometry

On SDS-PAGE, unfused rEcall migrated less rapidly than anticipated, thus a better estimate of mass was obtained via ESI/MS (Bobin et al., 2001). In Figure 25, the highlighted peak had a deconvoluted mass/charge ratio of 7538.4 m/z. If this value corresponds to removal of a hydrogen ion, a typical outcome in ESI/MS, then there is 99.3% agreement with the predicted molecular weight of 7591 Daltons.

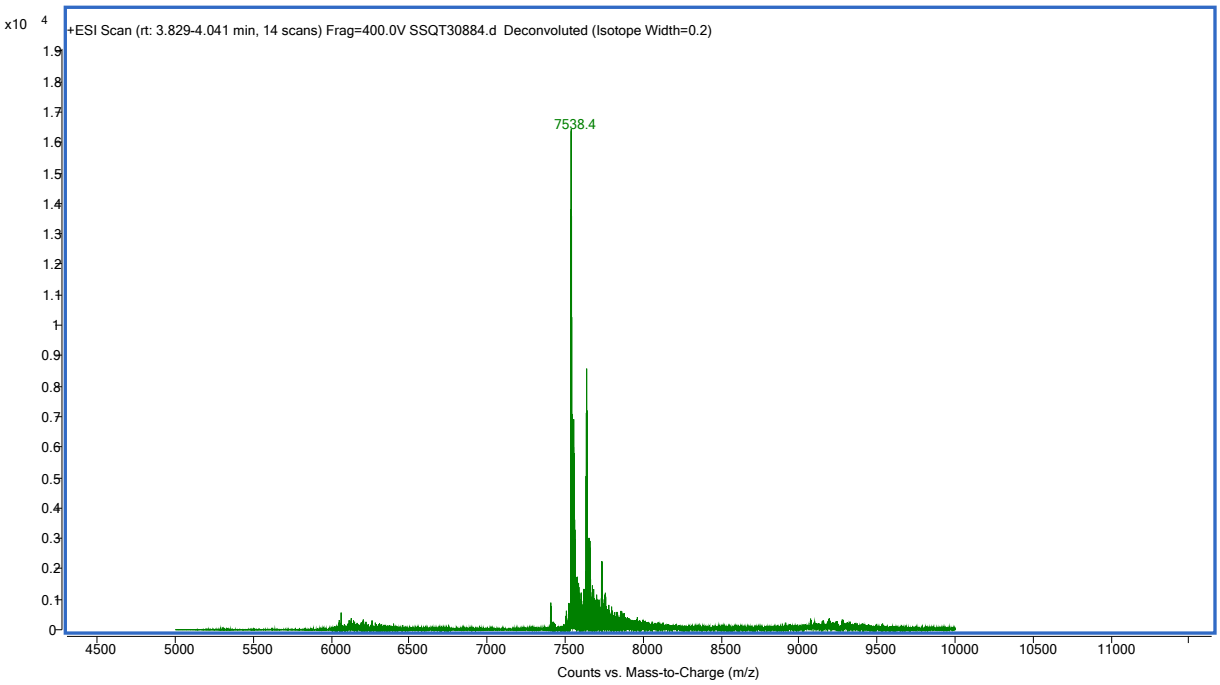

Figure 25: **Deconvoluted spectrum presenting the mass of H_6-rEcall.** The y-axis represents ion abundance, while x-axis represents the atomic mass (m/z).

4.0 Discussion

The central goal of this thesis project was to discover a novel protein that inhibits the contact pathway for extended periods, potentially providing a new therapeutic option for the treatment and prevention of HAE attacks. This was achieved by investigating the main hypothesis that fusing rEcall with HSA or ABD would prolong its half-life without altering its inhibitory properties towards PK. The orientation of the constructs was as follows; H_6-tag at the N- or C-terminus, rEcall, linker, and ABD at the C-terminus, or HSA at the N- or C-terminus. H_6-tag facilitated purification, and the linker created a buffer region between rEcall and HSA or ABD that could theoretically promote independent folding of the rEcall and fused domains.

4.1 HSA Position

HSA was placed at the N- or C-terminus to determine if the position of HSA impacts rEcall's behaviour *in vitro or in vivo*. In 2020, Ueda et al. provided an example for one particular combination of fused protein and HSA and found that HSA placement at the N-terminus was more effective in extending the fused protein half-life than placement of HSA at the C-terminus. This was evident as they fused Human lactoferrin (hLF), a globular protein that supports the innate immune system, with HSA to extend its life span. Two orientations were investigated, HSA-hLF and hLF-HSA. Data showed that HSA-hLF exhibited slower pharmacokinetic clearance; unfused hLF, hLF-HSA, and HSA-hLF had half-lives of 19.5, 64.0, and 403.6 mins, correspondingly (Ueda et al., 2020). Therefore, we tested this theory further by incorporating both H6-rEcall-HSA and HSA-rEcall-H6. Although this paper indicates that HSA at the N-terminus is more advantageous, rEcall-HSA was included because most HSA fusion proteins approved for clinical use were C-terminally tagged. Additionally, rEcall was fused to ABD as a

backup strategy, as literature denotes that ABD has a high affinity for both HSA and mouse serum albumin (MSA) (Nilvebrant & Hober, 2013). Thus, it was anticipated that producing rEcall recombinant proteins with the described orientations and compositions would provide fulsome information on the consequences of HSA fusion on rEcall function and clearance.

4.2 The Production of Recombinant Proteins

Constructs were engineered by digesting geneblocks or PCR products (Table 1). Next, restricting the desired cDNAs at their defined site enabled ligation and transformation into E. coli TOP 10 cells. All constructs were assembled using the same methods; Figures 6 &7 demonstrate the process of digesting, ligating and transforming H_6-rEcall. Sequences were confirmed using Sanger Sequencing, clones were then selected to be transformed into *Pichia pastoris* X-33 cells, expressed in 1-3L of BMMY, and purified via a nickel column. As presented in Table 2, H_6-rEcall, rEcall-H_6, H_6-rEcall-ABD, H_6-rEcall-HSA, HSA-rEcall-H_6, and HSA-H_6 yielded (in mg/liter of *P. pastoris* culture volume) 0.30 mg/L, 0.33 mg/L, 0.70 mg/L, 0.50 mg/L, 0.50 mg/L, and 4.7 mg/L, respectively. Recombinant HSA-H_6 was expressed to act as a control in the clearance experiments as a P. pastoris-derived protein previously demonstrated to be slowly cleared.

Also, GST and GST-RAP circular plasmids were transformed into E. coli BL21 cells. Post expression and purification, GST and GST-RAP yielded 23 and 1.5 mg/L, respectively. The purpose of expressing GST and GST-RAP was to determine the role LRP1 plays in rEcall degradation *in vivo*. Assessing LRP1 contribution was critical as rEcall is a TFPI variant, and TFPI is primarily degraded in the liver by LRP1 (Lillis et al., 2008).

Following protein purification, proteins were visualized on SDS PAGE, as shown in Figures 8 & 10. HSA fusion proteins were also visualized on immunoblots, Figure 9. According to Figure 8A, the SDS PAGE suggests that rEcall has a molecular weight of ~ 12 kDa, but the

literature points out that rEcall has a molecular weight of 7 kDa (Garnock-Jones, 2010). Because unfused rEcall migrated less rapidly than predicted, mass spectroscopy was performed. Mass was verified using electrospray ionization (ESI). Deconvolution of the spectrum indicated a species of MW 7538, Figure 25. The mass showed by mass spectroscopy is comparable to the one predicted by the amino acid sequence reported by the Clone software. Thus, it is verified that the size of unfused rEcall is consistent with the size reported in literature; ~ 7 kDa. Unfused rEcall likely does not migrate in SDS-PAGE as closely in proportion to its mass as larger proteins do because of its small size and atypical binding of less SDS per residue than other proteins.

4.3 Confirming Recombinant Proteins' Functionality

After confirming successful protein expressions in yeast, the activity of the recombinant proteins was examined in the presence of PK and increasing concentrations of PK-specific substrates. rEcall is a reversible competitive inhibitor of PK with a reported inhibition constant (K_i) of 25 pM; increasing concentrations of PK-specific substrates were expected to compete with rEcall proteins and bind to PK's active site (Markland et al., 1996). In this experiment, it was hypothesized that fusing rEcall with HSA or ABD would permit retention of rEcall's function. This was tested by plotting Michaelis-Menten and Lineweaver-Burk graphs to derive recombinant proteins' K_i values.

Figure 11 displays Michaelis-Menten graphs providing information surrounding the enzymatic reaction rate in the described conditions. Enzymatic reaction rates represent the rate at which substrates were cleaved in the presence of rEcall proteins. The graphs display reaction rates (mean V) against substrate concentrations (S2302) (Cornish-Bowden, 2015). In the absence of rEcall proteins, the Michaelis-Menten curve shows the typical PK interaction with its substrates. Initially, increasing levels of substrate concentrations increased reaction rates until it

reached a maximum value (Vmax). Vmax marked PK's active site saturation with substrates (Cornish-Bowden, 2015). In addition, increasing concentrations of H_6-rEcall, rEcall-H_6, H_6-rEcall-ABD, H_6-rEcall-HSA, or HSA-rEcall-H_6 altered the Michaelis-Menten curve. As anticipated, all five rEcall proteins hindered substrate cleavage by PK by blocking its active site; the shape of the curves was diagnostic of competitive inhibition. Increasing rEcall protein concentrations were proportional to PK inactivation, also supporting competitive inhibition.

Figures 12 & 13 show Lineweaver-Burk plots, linear transformations of the Michaelis-Menten curves. The slope of the reactions (1/S) is the same as the uninhibited reaction, but rEcall proteins changed the y-intercept (1/V) (Rodriguez et al., 2019). Increasing y-intercept represents the decrease in PK affinity for S2302. Lineweaver-Burk plots were created to determine proteins' K_i. Table 3 and Figures 11-14 prove that all five proteins had comparable K_i values of ~ 2 – 3 nM, suggesting that modifications to rEcall did not impact its primary function, which is PK inactivation.

Previous reports indicated that clinical grade Ecallantide has a K_i value of 25 pM (Garnock -Jones, 2010). While this form of Ecallantide was also produced in *Pichia pastoris*, it lacked a hexahistidine tag. It is not entirely clear why the current K_i values do not align with the previous value of 25 pM, however some of this uncertainty arises because methods and data supporting the established K_i are not available in the public literature. Efforts to obtain clinical grade Ecallantide from the manufacturer were unsuccessful, and the product cannot be purchased in Canada.

4.4 rEcall Proteins Hindering PK's Multifunction

As mentioned in the Introduction, PK plays various roles in the coagulation cascade, including cleaving FXII and HK. In 2021, Kearney et al. revealed a novel PK function, which

was to cleave and activate FIX. Thus, to further support the kinetics of rEcall proteins, an additional experiment was incorporated. rEcall proteins' ability to inhibit PK from cleaving its macromolecular targets (HK, FXII, and FIX) was assessed. Cleavage assays were conducted and visualized on SDS PAGE (Figures 15-17). As expected, at 37 °C for 1 hour, PK fully cleaved its substrates (HK, FXII, and FIX). Conversely, the cleavage of proteases by PK was blocked by introducing H_6-rEcall, H_6-rEcall-ABD, or H_6-rEcall-HSA to the reactions. The three recombinant proteins diminished PK activity at identical rates. This conclusion was derived from analyzing full and partial inhibition of PK. rEcall-modified proteins cleaved proteases similarly and displayed bands with indistinguishable intensities under analogous conditions. rEcall proteins, fused or unfused to HSA or ABD, and with hexahistidine tags in different positions, inhibited PK proteolysis of both small synthetic substrates and large macromolecular natural substrates.

4.5 Confirming Specificity For PK

Pharmaceutical companies manufacturing Ecallantide, such as Takeda Pharmaceuticals, claim that it is specific for PK (Maurer et al., 2022). Because protease inhibitors rarely exhibit absolute specificity, rEcall's specificity was evaluated. Figures 18 & 19 present recombinant proteins' specificity for PK by observing their ability to interact with other serine proteases, including FXIIa, FXIa, FIXa, FIIa, and PLSN. It was predicted that rEcall proteins would have some anti-PLSN activity, as this was established in the first studies of TFPI phage display libraries in which Ecallantide was developed (Markland et al., 1996). Results suggests that rEcall proteins inhibit PLSN, but PK inactivation is more substantial. Furthermore, FXI minor inactivation by rEcall-modified proteins was unforeseen, as it is not documented in the literature or specified by manufacturers. Nevertheless, the kinetic experiments indicate that the primary

function of H_6-rEcall, H_6-rEcall-HSA, rEcall-H_6, and HSA-rEcall-H_6 was to diminish PK activity.

4.6 Previous HSA Fusions

The Sheffield laboratory has engineered various HSA fusion proteins. Analogous to rEcall, proteins investigated played a role in coagulation and had short half-lives and brief plasma residency profiles; proteins as hirudin (Syed et al., 1997), barbourin (Marques et al., 2001), and KPI (Sheffield et al., 2018). Studies conducted showed that proteins fused with HSA maintained their primary function while elongating the half-life by up to 5 days in rabbits. In murine models, the Sheffield lab reported the clearance profiles of KPI and KPI-HSA after 30 minutes of injection. 17 ± 1% of KPI vs. 77 ± 2% of KPI-HSA remained in the circulation ($p < 0.05$ vs. KPI). Therefore, it was anticipated that H_6-rEcall-HSA and H_6-rEcall-ABD will behave as fused KPI in vivo, as KPI contains a Kunitz domain, similar to rEcall (Sheffield et al., 2018).

Albumin fusion is believed to extend the clearance of small proteins by resisting glomerular filtration and undergoing recycling via FcRn. Strikingly, 2 hours post-injection, 26 ± 2 % of H_6-rEcall-HSA remained in circulation vs. 7 ± 1% of H_6-rEcall-ABD and 6 ± 2 % of H_6-rEcall ($p < 0.0001$). Figure 20 shows that fusion to albumin prolonged rEcall's plasma residency time, but it was less substantial than expected based on the KPI example cited above. Clearance of H_6-rEcall-HSA in vivo was ~4-fold slower than H_6-rEcall, an effect less than that observed for similar fusion proteins, as KPI-HSA. It was hypothesized that constraint on half-life extension arose from the position of the hexahistidine tag or the relative position of rEcall and HSA domains.

It was speculated that fusing HSA to the C-terminus of rEcall may have resulted in steric hindrance or allosteric effects and prevented more substantial rEcall half-life extension.

Therefore, to further investigate rEcall fused to HSA, HSA-rEcall-H_6 was engineered. As a control for slow clearance, HSA-H_6 was also injected (n=6). Figure 21 demonstrates that fusing albumin to the N- or C-terminal of rEcall led to similar clearance profiles in vivo. Two hours after injection, 50 ± 10% of H_6-rEcall-HSA remained in the circulation vs. 12 ± 3 % of rEcall-H_6 ($p < 0.0001$). Additionally, 36 ± 6 % of HSA-rEcall-H_6 remained vs. 75 ± 5% of HSA-H_6 ($p < 0.0001$) (Figure 21). These data indicate that rEcall fusion proteins were eliminated more rapidly than HSA- H_6 expressed and purified in the same system regardless of the placement of HSA or H_6 at the C- or N-terminus. In comparison to the fusion proteins, rEcall- H_6 presented the fastest clearance rate, as predicted.

HSA has three domains, and mutagenic studies have shown that the regions responsible for the interaction with FcRn are the C-terminal domain III with additional help from the N-terminal domain I (Andersen et al., 2012). These regions may be affected by the attachment of rEcall to HSA. In addition, the shorter half-life of HSA in mice is attributed to murine FcRn not recognizing HSA as avidly as MSA (Andersen et al., 2010). Andersen et al. found a terminal half-life for HSA in mice of 21 hours, considerably shorter than the half-life of HSA in humans, 19 days.

4.7 Factors Affecting the Ability of ABD to Form A Complex with Albumin

As for H_6-rEcall-ABD, the rate of clearance was analogous to unfused rEcall. Perhaps, the addition of ABD caused steric hindrance impacting its affinity for albumin, Figures 20 & S2. The reason ABD was positioned at the C-terminus was for consistency purposes, as HSA was placed at C-terminus. Also, the affinity for HSA and MSA may be not as strong as documented. Li et al. have reported that N-terminally tagging proteins with ABD are superior to ABD at the C-terminus. Li et al. attached ABD to human tumour necrosis factor-related apoptosis-inducing

ligand (hTRAIL) at the N- or C-terminus. It was reported that ABD-hTRAIL had a high affinity for HSA (K_D of 0.4 ± 0.18 nM), although literature proposes that ABD has a significantly stronger affinity for HSA, with K_D of 120 fM (Nilvebrant & Hober, 2013). In addition, ABD-hTRAIL formed a complex with MSA and prolonged the half-life of hTRAIL by 50-fold. Whereas hTRAIL-ABD did not display an affinity for albumin, hence failing to extend the half-life of hTRAIL. Therefore, the placement of ABD may be responsible for the loss of affinity for HSA and MSA.

4.8 Receptors Responsible For Proteins Clearance

Small proteins are typically filtered from the blood in the kidneys and depart from the body via this renal route unless they are ligands for specific receptors (Sheffield et al., 2001). The catabolism of many plasma proteins is mediated via LRP1, a multifunctional surface receptor found on hepatocytes that degrades captured proteins via endocytosis (Gonias et al., 2004). In 1994, Warshawsky and colleagues reported that LRP1 controls TFPI clearance. *In vivo*, they observed the clearance profile of ^{125}I-TFPI in the presence of RAP, a 39 kDa protein that acts as an LRP1 antagonist. Mice overexpressing RAP exhibited reduced plasma ^{125}I -TFPI degradation. It is evident that a different clearance mechanism moderates fused and unfused rEcall degradation, as HSA-H_6 was much less rapidly cleared, as anticipated (Figures 20 & 21). rEcall is primarily made up of the first Kunitz domain of TFPI, and possibly the same clearance mechanism is responsible for rEcall and TFPI terminal catabolism. To test the theory that indicates the presence of an alternate pathway responsible for rEcall fusions' clearance, competition experiments were performed.

Competition experiments included the co-administration of H_6-rEcall-HSA with GST, GST-RAP, or IVIg. Experiments showed that GST-RAP, but not GST alone, slowed the

clearance of H_6-rEcall-HSA by blocking LRP1 binding. This finding suggests that unfused rEcall is cleared predominantly via LRP1 and that rEcall fusion to HSA only partly counteracts this powerful interaction. It is also possible that the seven novel amino acid mutations introduced into the first Kunitz domain of TPFI to generate Ecallantide enhanced its binding affinity to LRP1 versus native soluble TFPI (Markland et al., 1996).

Similar to albumin, IgG is known to possess a long circulatory half-life because it also undergoes recycling via FcRn (Sleep, 2013). To determine if FcRn contributed to the small but significant prolongation of rEcall clearance associated with albumin, IVIg was used as a competitor of ^{125}I-labelled H_6-rEcall-HSA clearance. The results signified that H_6-rEcall-HSA clearance was partially blocked. IVIg blockade spares platelets from clearance and destruction in immune thrombocytopenia, and a similar partial sparing of H_6-rEcall-HSA was noted (Blumberg et al., 2019). It is not clear why blocking H_6-rEcall-HSA binding to FcRn would not deflect it to the LRP1 route, but it is possible that this phenomenon would have been observed had our experiments been of longer duration. The time course of the experiment was short in that H_6-rEcall-HSA was injected, and blood samples were obtained at 2 and 30 mins. The duration of the experiment may have been significant, as the relative kinetics of LRP1 and FcRn interaction are not well established. Perhaps during the 30 minutes, IgG blocked FcRn leaving more H_6-rEcall-HSA in the circulation, and some proteins were internalized and to be recycled. According to the data obtained, LRP1 may be a higher affinity receptor compared to FcRn as LRP1 blockage presented a longer half-life extension of H_6-rEcall-HSA. Taken together, both LRP1 and FcRn contribute to H_6-rEcall-HSA clearance; however, LRP1 plays a greater role in H_6-rEcall-HSA clearance than FcRn.

To further verify the theory that denotes rEcall is predominantly degraded by the liver and not the kidneys, protein distribution in mice was conducted by cannulating the jugular vein and delivering ^{125}I-labelled-HSA-rEcall-H_6 or ^{125}I-labelled rEcall- H_6. Post-mortem, organs were extracted and analyzed. Figure 24 shows that unfused rEcall is mainly found in the kidneys, and HSA-rEcall-H_6 is in the liver. It was expected that unfused rEcall would be primarily cleared by the kidneys as it has a size of 7 kDa, which meets the glomerular filtration limit. The filtration limit is the size restriction enforced by the glomerular filtration barrier in the kidneys. In the kidneys, there are specialized capillaries called glomerular capillaries. It is within these capillaries, the glomerular filtration barrier acts as a filter that allows selected substances to pass through to be excreted in the urine. The filtration limit is determined by the charge and size of proteins; the limit is approximately 60 kDa (Saritas et al., 2015). Moreover, it was speculated that rEcall associated with HSA may be redirected to the liver as the co-injection of H_6-rEcall-HSA with GST-RAP extended its circulation periods in the competition experiment. Overall, the competition and organ distribution experiments together indicated that H_6-rEcall-HSA is eliminated from the bloodstream by the liver rather than the kidneys. This observation partly explains why rEcall fused to HSA did not prolong its half-life as significantly as predicted.

5.0 Conclusion

In vitro, unfused and fused rEcall proteins behaved similarly, as hypothesized. In vivo, unfused rEcall proteins were rapidly cleared. Fusion proteins combining rEcall with HSA in two orientations (H_6-rEcall-HSA or HSA-rEcall-H_6) cleared less rapidly than unfused rEcall, but not by the wide margin observed with other HSA fusion proteins. The relatively minor half-life

elongation of rEcall by HSA likely arises due to the dominant role of LRP1 in the clearance and catabolism of fused and unfused rEcall, an interaction that significantly overpowers FcRn recycling.

6.0 Limitations

A limitation of this study was that we did not test the functionality of rEcall fusion proteins in vivo. Although fusion proteins exhibited partial pharmacokinetic enhancements, their activity in vivo remains undetermined. It is critical to verify that rEcall proteins inactivate mouse PK as effectively as human PK. Papers suggest that the co-injection of Ecallantide with other PK inhibitors hinders PK function in mice. However, can rEcall and its modified proteins independently inhibit mouse PK? Also, the exact mechanism in which rEcall inhibits mouse or human PK is unknown, or not available in the public literature. Therefore, a follow-up study could address these unanswered questions.

Another more specific limitation is that we needed to radiolabel rEcall proteins to follow their clearance from the murine plasma after intravenous injection. Radiolabeling with radioactive sodium iodide is a chemical modification that leaves the tyrosine residues of the treated protein permanently altered and can affect labeled protein structure and function. rEcall contains 3 tyrosine residues and HSA contains 18. It is likely that a greater degree of modification could yield to a less naturally conformation of labeled proteins than a lesser degree. In that regard, the experiments shown in Figure 20 involved proteins labeled for a longer reaction time (5 minutes) than those shown in Figure 21 (1 minute). Longer-reacted H_6-rEcall-HSA had a

mean AUC of 250 ± 10 %-hours while lesser-reacted H_6-rEcall-HSA had a mean AUC of 620 ± 50 %-hours, consistent with the possibility that too high a density of tyrosine modifications could affect clearance. Wherever possible, comparisons have been made to lesser-reacted, more native-like material. Had we had access to a high affinity monoclonal antibody reacting with rEcall, we could have avoided radiolabeling entirely, but none were commercially available.

7.0 Future Directions

A way to identify the activity of rEcall proteins is through the use of Evans Blue Dye in C1INH-deficient mice (Yao et al., 2018). Evans Blue Dye is a synthetic dye that has a deep blue colour. It is used as a marker for plasma volume and vascular permeability. With respect to vascular permeability, the blue dye leaks out of the blood vessels and accumulates in the extravascular space. This results in changing the colour of the skin to blue, which indicates inflammation and fluid leakage (Qiu et al., 2019). Previously, it has been reported that PK inhibitor (DX88), Ecallantide, reversed vascular permeability in C1INH-deficient mice (Han et al., 2002). Thus, Evans Blue Dye in C1INH-deficient mice could reveal whether or not rEcall proteins behave as unfused rEcall, in vivo.

Another method to identify the activity of the fusion proteins is by detecting BK levels in cardiac atrial tissue, blood, and urine. This can be accomplished by carrying out high-performance liquid chromatography (HPLC)-based radioimmunoassays to measure bradykinin levels in plasma post-injection of recombinant proteins (Campbell et al., 2001).

It is also important to identify a reversal agent for Ecallantide, as it is administered to patients aged ≥ 12 years. In the rare scenarios where young individuals fail to tolerate 30 mg of

Ecallantide, it might be useful to have a reversal agent available. A potential reversal agent could be Angiotensin-converting enzyme inhibitors (ACEI) (Baram et al., 2013). In normal conditions, ACE is a vasoconstrictor that breaks down bradykinin and prevents inflammation. Therefore, ACEI decrease blood pressure by promoting vasodilation and BK accumulation (Vasekar & Craig, 2012).

Moreover, results obtained in this study suggest that the addition of ABD to the C-terminus of a small protein, as rEcall, fails to drive complex formation with albumin. It would be interesting to examine fusing a small protein with ABD at the N-terminus and determine if a hypothesis that signifies that ABD is only functional at N- and not the C-terminus of proteins is supported.

Finally, it would be beneficial to analyze the immunogenicity of rEcall and its proteins. This is possible by obtaining plasma post-injection and conducting T cell proliferation, cytokine release, or binding assays [enzyme-linked immunosorbent assay (ELISA)] (Jahn & Schneider, 2009). These assays reveal if the immune system was triggered after the injection of rEcall proteins. rEcall proteins could also be re-administered over time and ELISAs performed to address if chronic use leads to anti-drug antibody formation.

Appendix

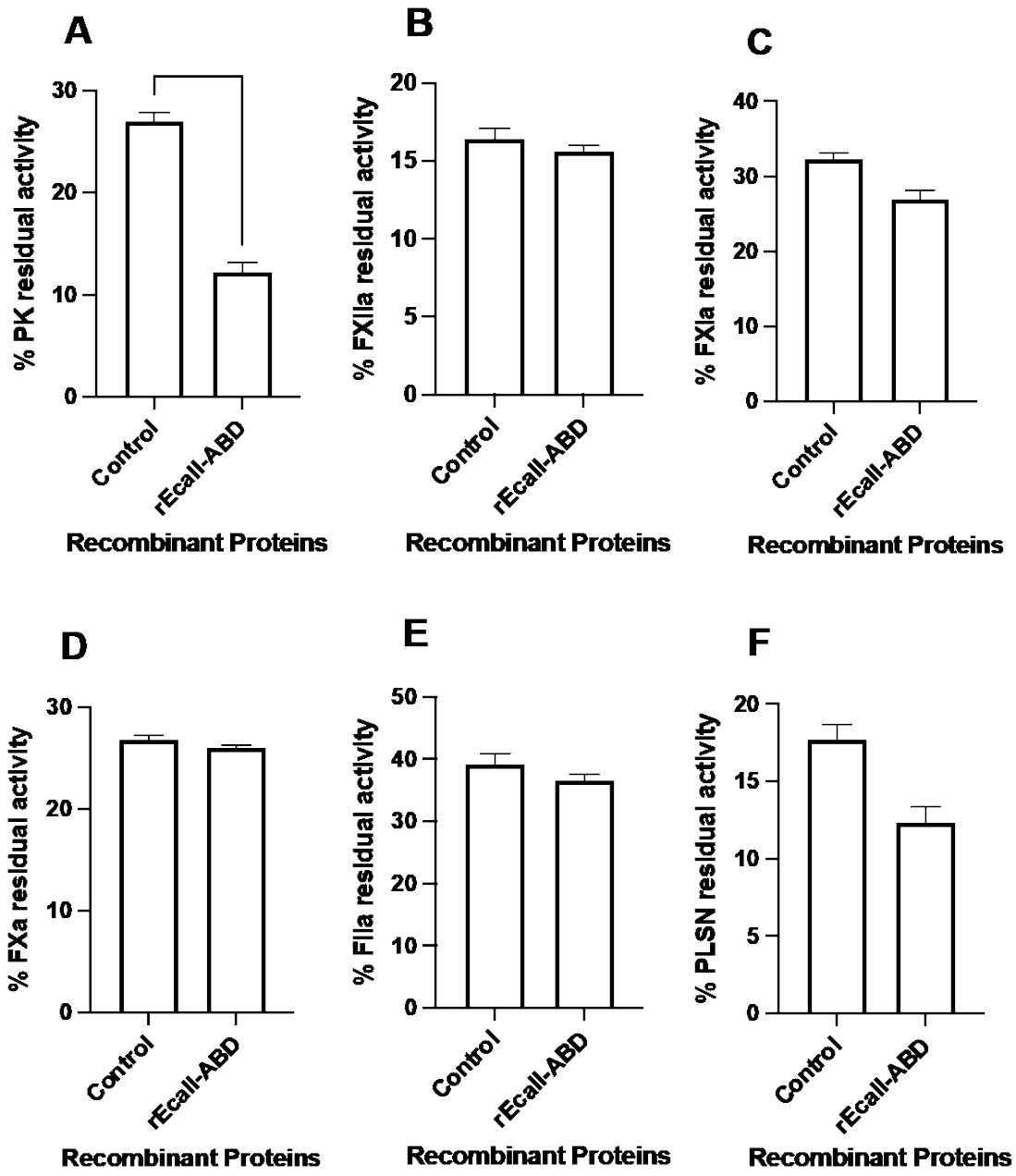

Figure S1: Assessing the specificity of H_6-rEcall-ABD for PK. The residual activity is obtained by observing proteases' ability to bind and cleave their respective chromogenic substrates (n=5, * $p<0.05$, ** $p<0.01$, *** $p<0.001$, **** $p<0.0001$).

Figure S2: Examining the binding of H_6-rEcall-ABD to HSA through immunoprecipitation reactions. The absence of a component is illustrated by "-" and the presence by "+". Reactions were electrophoresed on a 15% SDS PAGE.

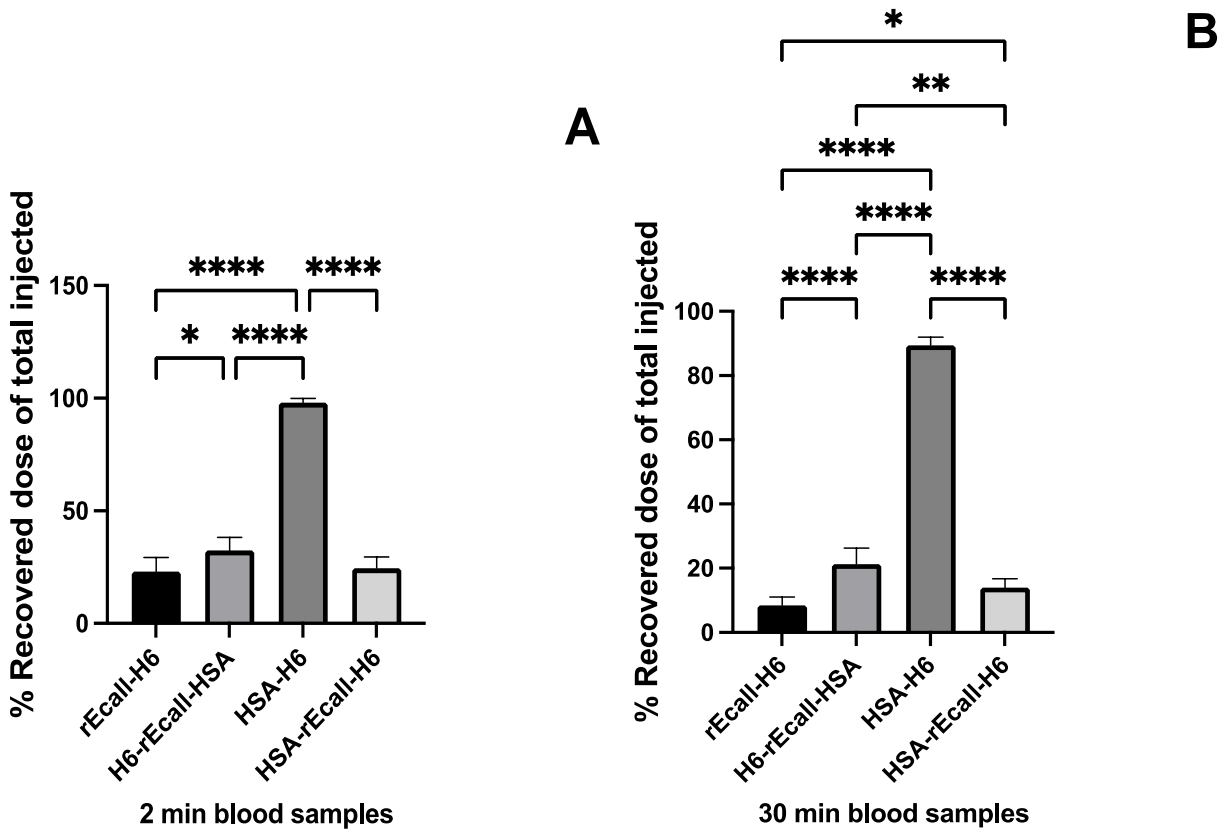

Figure S3: Radiolabeled protein recovery 2 and 30 mins after injection. ^{125}I-labelled proteins observed were rEcall- H_6, H_6-rEcall-HSA, HSA-H_6, and HSA-rEcall-H_6 (identified on the x-axis). The y-axis represents the % protein recovered of the total amount injected A) after 2 mins and B) after 30 mins. Statistical comparisons between groups identified by horizontal brackets are indicated by * $p<0.05$, ** $p<0.01$, *** $p<0.001$, **** $p<0.0001$.

References:

1. Andersen, J. T., Dalhus, B., Cameron, J., Daba, M. B., Plumridge, A., Evans, L., ... & Sandlie, I. (2012). Structure-based mutagenesis reveals the albumin-binding site of the neonatal Fc receptor. Nature communications, 3(1), 610.
2. Andersen, J. T., Daba, M. B., Berntzen, G., Michaelsen, T. E., & Sandlie, I. (2010). Cross-species Binding Analyses of Mouse and Human Neonatal Fc Receptor Show Dramatic Differences in Immunoglobulin G and Albumin Binding 2. Journal of Biological Chemistry, 285(7), 4826-4836
3. Baram, M., Kommuri, A., Sellers, S. A., & Cohn, J. R. (2013). ACE inhibitor–induced angioedema. The Journal of Allergy and Clinical Immunology: In Practice, 1(5), 442-445
4. Bernstein, J. A. (2018). Severity of hereditary angioedema, prevalence, and diagnostic considerations. Am J Manag Care, 24(14 Suppl), S292-S298
5. Bradford, M. M. (1976). A rapid and sensitive method for the quantitation of microgram quantities of protein utilizing the principle of protein-dye binding. Analytical biochemistry, 72(1-2), 248-254.
6. Bhakta, V., Hamada, M., Nouanesengsy, A., Lapierre, J., Perruzza, D. L., & Sheffield, W. P. (2021). Identification of an alpha-1 antitrypsin variant with enhanced specificity for factor XIa by phage display, bacterial expression, and combinatorial mutagenesis. Scientific Reports, 11(1), 1-14.
7. Björkqvist, J., Jämsä, A., & Renné, T. (2013). Plasma kallikrein: the bradykinin-producing enzyme. Thrombosis and haemostasis, 110(09), 399-407.
8. Blumberg, L. J., Humphries, J. E., Jones, S. D., Pearce, L. B., Holgate, R., Hearn, A., ... & Blumberg, R. S. (2019). Blocking FcRn in humans reduces circulating IgG levels and inhibits IgG immune complex–mediated immune responses. Science Advances, 5(12), eaax9586
9. Bobin, S., Popot, M. A., Bonnaire, Y., & Tabet, J. C. (2001). Approach to the determination of insulin-like-growth-factor-I (IGF-I) concentration in plasma by high-performance liquid chromatography-ion trap mass spectrometry: use of a deconvolution algorithm for the quantification of multiprotonated molecules in electrospray ionization. Analyst, 126(11), 1996-2001
10. Broos, K., Feys, H. B., De Meyer, S. F., Vanhoorelbeke, K., & Deckmyn, H. (2011). Platelets at work in primary hemostasis. Blood reviews, 25(4), 155-167
11. Broze Jr, G. J., & Girard, T. J. (2012). Tissue factor pathway inhibitor: structure-function. Front Biosci, 17(1), 262-280.
12. Callis, J. (1995). Regulation of protein degradation. The plant cell, 7(7), 845.
13. Canadian Blood Services. (2022). Plasma donation: What you need to know. Retrieved from https://www.blood.ca/sites/default/files/F802238_2022-02-09.pdf
14. Canadian Blood Services. (2019). CBS annual report 2019. Retrieved from https://annual2019.blood.ca/pdfs/CBS-AR2019-en.pdf
15. Campbell, D. J. (2001). The kallikrein–kinin system in humans. Clinical and experimental pharmacology and physiology, 28(12), 1060-1065
16. Cornish-Bowden, A. (2015). One hundred years of Michaelis–Menten kinetics. Perspectives in Science, 4, 3-9.

17. Costa-Neto, C. M., Dillenburg-Pilla, P., Heinrich, T. A., Parreiras-e-Silva, L. T., Pereira, M. G., Reis, R. I., & Souza, P. P. (2008). Participation of kallikrein–kinin system in different pathologies. International immunopharmacology, 8(2), 135-142.
18. Cicardi, M., Levy, R. J., McNeil, D. L., Li, H. H., Sheffer, A. L., Campion, M., ... & Pullman, W. E. (2010). Ecallantide for the treatment of acute attacks in hereditary angioedema. New England Journal of Medicine, 363(6), 523-531.
19. Cichon, S., Martin, L., Hennies, H. C., Müller, F., Van Driessche, K., Karpushova, A., ... & Nöthen, M. M. (2006). Increased activity of coagulation factor XII (Hageman factor) causes hereditary angioedema type III. The American Journal of Human Genetics, 79(6), 1098-1104
20. Cruz, M. P. (2015). Conestat alfa (ruconest): first recombinant c1 esterase inhibitor for the treatment of acute attacks in patients with hereditary angioedema. Pharmacy and Therapeutics, 40(2), 109.
21. Cugno, M., & Tedeschi, A. (2014). Coagulation factor autoantibodies. In Autoantibodies (pp. 499-509). Elsevier
22. Dahlbäck, B. (2000). Blood coagulation. The Lancet, 355(9215), 1627-1632
23. De Maat, S., cofman, Z. L. M., & Maas, C. (2018). Hereditary angioedema: the plasma contact system out of control. Journal of Thrombosis and Haemostasis, 16(9), 1674-1685.
24. Dobó, J., Major, B., Kékesi, K. A., Szabó, I., Megyeri, M., Hajela, K., ... & Gál, P. (2011). Cleavage of kininogen and subsequent bradykinin release by the complement component: mannose-binding lectin-associated serine protease (MASP)-1. PloS one, 6(5), e20036.
25. Dorgalaleh, A., Daneshi, M., Rashidpanah, J., & Roshani Yasaghi, E. (2018). An overview of hemostasis. Congenital Bleeding Disorders: Diagnosis and Management, 3-26
26. D'souza, A. A., & Shegokar, R. (2016). Polyethylene glycol (PEG): a versatile polymer for pharmaceutical applications. Expert opinion on drug delivery, 13(9), 1257-1275
27. Eweas, A. F., Maghrabi, I. A., & Namarneh, A. I. (2014). Advances in molecular modeling and docking as a tool for modern drug discovery. Der Pharma Chemica, 6(6), 211-228.
28. Ferguson, M. A., & Waikar, S. S. (2012). Established and emerging markers of kidney function. Clinical chemistry, 58(4), 680-689
29. Fraker, P. J., & Speck Jr, J. C. (1978). Protein and cell membrane iodinations with a sparingly soluble chloroamide, 1, 3, 4, 6-tetrachloro-3a, 6a-diphenylglycoluril. Biochemical and biophysical research communications, 80(4), 849-857.
30. Frejd, F. Y. (2012). Half-life extension by binding to albumin through an albumin binding domain. Therapeutic proteins: strategies to modulate their plasma half-lives, 269-283.
31. Garnock-Jones, K. P. (2010). Ecallantide. Drugs, 70(11), 1423-1431.
32. Gill, S. C., & Von Hippel, P. H. (1989). Calculation of protein extinction coefficients from amino acid sequence data. Analytical biochemistry, 182(2), 319-326
33. Gonias, S. L., Wu, L., & Salicioni, A. M. (2004). Low density lipoprotein receptor-related protein: regulation of the plasma membrane proteome. Thrombosis and haemostasis, 91(06), 1056-1064.

34. Gordon, S. (2007). The macrophage: past, present and future. European journal of immunology, 37(S1), S9-S17
35. Guo, R., Guo, W., Cao, L., Liu, H., Liu, J., Xu, H., ... & Hong, Z. (2016). Fusion of an albumin-binding domain extends the half-life of immunotoxins. International Journal of Pharmaceutics, 511(1), 538-549.
36. Hahn, J., Trainotti, S., Wigand, M. C., Schuler, P. J., Hoffmann, T. K., & Greve, J. (2020). Prospective Analysis in Patients with HAE Under Prophylaxis With Lanadelumab: A Real-life Experience. Journal of Drugs in Dermatology: JDD, 19(10), 978-983
37. Han, E. D., MacFarlane, R. C., Mulligan, A. N., Scafidi, J., & Davis, A. E. (2002). Increased vascular permeability in C1 inhibitor–deficient mice mediated by the bradykinin type 2 receptor. The Journal of clinical investigation, 109(8), 1057-1063
38. He, Z., Wang, G., Wu, J., Tang, Z., & Luo, M. (2021). The molecular mechanism of LRP1 in physiological vascular homeostasis and signal transduction pathways. Biomedicine & Pharmacotherapy, 139, 111667
39. Jahn, E. M., & Schneider, C. K. (2009). How to systematically evaluate immunogenicity of therapeutic proteins–regulatory considerations. New biotechnology, 25(5), 280-286
40. Kalinska, M., Meyer-Hoffert, U., Kantyka, T., & Potempa, J. (2016). Kallikreins–the melting pot of activity and function. Biochimie, 122, 270-282.
41. Karbalaei, M., Rezaee, S. A., & Farsiani, H. (2020). Pichia pastoris: A highly successful expression system for optimal synthesis of heterologous proteins. Journal of cellular physiology, 235(9), 5867-5881.
42. Kayashima, Y., Smithies, O., & Kakoki, M. (2012). Kinins—the kallikrein-kinin system and oxidative stress. Current opinion in nephrology and hypertension, 21(1), 92
43. Kearney, K. J., Butler, J., Posada, O. M., Wilson, C., Heal, S., Ali, M., ... & Philippou, H. (2021). Kallikrein directly interacts with and activates Factor IX, resulting in thrombin generation and fibrin formation independent of Factor XI. Proceedings of the National Academy of Sciences, 118(3), e2014810118.
44. Kobayashi, K. (2006). Summary of recombinant human serum albumin development. Biologicals, 34(1), 55-59. Lee, A. (2021). Berotralstat: First Approval. Drugs, 1-5.
45. Kontermann, R. E. (2011). Strategies for extended serum half-life of protein therapeutics. Current opinion in biotechnology, 22(6), 868-87
46. Kuo, T. T., Baker, K., Yoshida, M., Qiao, S. W., Aveson, V. G., Lencer, W. I., & Blumberg, R. S. (2010). Neonatal Fc receptor: from immunity to therapeutics. Journal of clinical immunology, 30, 777-789
47. Latvala, S., Jacobsen, B., Otteneder, M. B., Herrmann, A., & Kronenberg, S. (2017). Distribution of FcRn across species and tissues. Journal of Histochemistry & Cytochemistry, 65(6), 321-333.
48. Li, R., Yang, H., Jia, D., Nie, Q., Cai, H., Fan, Q., ... & Lu, X. (2016). Fusion to an albumin-binding domain with a high affinity for albumin extends the circulatory half-life and enhances the in vivo antitumor effects of human TRAIL. Journal of Controlled Release, 228, 96-106.
49. Lillis, A. P., Van Duyn, L. B., Murphy-Ullrich, J. E., & Strickland, D. K. (2008). LDL receptor-related protein 1: unique tissue-specific functions revealed by selective gene knockout studies. Physiological reviews, 88(3), 887-918.

50. Longhurst, H., Cicardi, M., Craig, T., Bork, K., Grattan, C., Baker, J., ... & Zuraw, B. L. (2017). Prevention of hereditary angioedema attacks with a subcutaneous C1 inhibitor. New England journal of medicine, 376(12), 1131-1140
51. Longtine, M. S., Mckenzie III, A., Demarini, D. J., Shah, N. G., Wach, A., Brachat, A., ... & Pringle, J. R. (1998). Additional modules for versatile and economical PCR-based gene deletion and modification in Saccharomyces cerevisiae. Yeast, 14(10), 953-961
52. Lunn, M., & Banta, E. (2011). Ecallantide for the treatment of hereditary angiodema in adults. Clinical Medicine Insights: Cardiology, 5, CMC-S4434.
53. Mannuccio, P. M. (2015). Half-life extension technologies for haemostatic agents. Thrombosis and haemostasis, 113(01), 165-176
54. Maurer, M., Magerl, M., Betschel, S., Aberer, W., Ansotegui, I. J., Aygören-Pürsün, E., … & Craig, T. (2022). The international WAO/EAACI guideline for the management of hereditary angioedema–The 2021 revision and update. World Allergy Organization Journal, 15(3), 100627.
55. Markland, W., Ley, A. C., & Ladner, R. C. (1996). Iterative optimization of high-affinity protease inhibitors using phage display. 2. Plasma kallikrein and thrombin. Biochemistry, 35(24), 8058-8067.
56. Maroney, S. A., & Mast, A. E. (2015). New insights into the biology of tissue factor pathway inhibitor. Journal of Thrombosis and Haemostasis, 13, S200-S207
57. Marques, J. A., George, J.K., Smith, I.J., Bhakta, V., Sheffield, W.P (2001). A barbourin-albumin fusion protein that is slowly cleared in vivo retains the ability to inhibit platelet aggregation in vitro. Thromb Haemost. 2001 Sep;86(3):902-8.
58. Martinez-Vicente, M., Sovak, G., & Cuervo, A. M. (2005). Protein degradation and aging. Experimental gerontology, 40(8-9), 622-633
59. McMichael, M. (2005). Primary hemostasis. Journal of veterinary emergency and critical care, 15(1), 1-8
60. Moldave, K. (1985). Eukaryotic protein synthesis. Annual review of biochemistry, 54(1), 1109-1149
61. Moreau, M. E., Garbacki, N., Molinaro, G., Brown, N. J., Marceau, F., & Adam, A. (2005). The kallikrein-kinin system: current and future pharmacological targets. Journal of pharmacological sciences, 99(1), 6-38.
62. Narita, M., Bu, G., Olins, G. M., Higuchi, D. A., Herz, J., Broze, G. J., & Schwartz, A. L. (1995). Two Receptor Systems Are Involved in the Plasma Clearance of Tissue Factor Pathway Inhibitor in Vivo (∗). Journal of Biological Chemistry, 270(42), 24800-24804
63. Norris, L. A. (2003). Blood coagulation. Best Practice & Research Clinical Obstetrics & Gynaecology, 17(3), 369-383.
64. Nilvebrant, J., & Hober, S. (2013). The albumin-binding domain as a scaffold for protein engineering. Computational and structural biotechnology journal, 6(7), e201303009
65. Nzeako, U. C., Frigas, E., & Tremaine, W. J. (2001). Hereditary angioedema: a broad review for clinicians. Archives of Internal Medicine, 161(20), 2417-2429.
66. Oganesyan, V., Damschroder, M. M., Cook, K. E., Li, Q., Gao, C., Wu, H., & Dall'Acqua, W. F. (2014). Structural insights into neonatal Fc receptor-based recycling mechanisms. Journal of Biological Chemistry, 289(11), 7812-7824
67. Palta, S., Saroa, R., & Palta, A. (2014). Overview of the coagulation system. Indian journal of anaesthesia, 58(5), 515

68. Pathak, M., Wong, S. S., Dreveny, I., & Emsley, J. (2013). Structure of plasma and tissue kallikreins. Thrombosis and haemostasis, 110(09), 423-433.
69. Ponczek, M. B. (2021). High molecular weight Kininogen: a review of the structural literature. International Journal of Molecular Sciences, 22(24), 13370
70. Poppelaars, F., Damman, J., de Vrij, E. L., Burgerhof, J. G. M., Saye, J., Daha, M. R., ... & Seelen, M. A. (2016). New insight into the effects of heparinoids on complement inhibition by C1-inhibitor. Clinical & Experimental Immunology, 184(3), 378-388.
71. Powell, J., Piszczatoski, C., & Rubido, E. (2022). Orladeyo (Berotralstat): A Novel Oral Therapy for the Prevention of Hereditary Angioedema. Annals of Pharmacotherapy, 56(4), 488-493.
72. Pyzik, M., Kozicky, L. K., Gandhi, A. K., & Blumberg, R. S. (2023). The therapeutic age of the neonatal Fc receptor. Nature Reviews Immunology, 1-18
73. Qiu, T., Chiuchiolo, M. J., Whaley, A. S., Russo, A. R., Sondhi, D., Kaminsky, S. M., ... & Pagovich, O. E. (2019). Gene therapy for C1 esterase inhibitor deficiency in a murine model of hereditary angioedema. Allergy, 74(6), 1081-1089.
74. Rodriguez, J. M. G., Hux, N. P., Philips, S. J., & Towns, M. H. (2019). Michaelis–Menten graphs, Lineweaver–Burk plots, and reaction schemes: Investigating introductory biochemistry students' conceptions of representations in enzyme kinetics. Journal of Chemical Education, 96(9), 1833-1845.
75. Riedl, M. A. (2013). Hereditary angioedema with normal C1-INH (HAE type III). The Journal of Allergy and Clinical Immunology: In Practice, 1(5), 427-432
76. Riedl, M. (2010). Hereditary angioedema therapy: Kallikrein inhibition and bradykinin receptor antagonism. World Allergy Organization Journal, 3(3), S34-S38.
77. Roopenian, D. C., & Akilesh, S. (2007). FcRn: the neonatal Fc receptor comes of age. Nature reviews immunology, 7(9), 715-725.
78. Samis, J. A., Ramsey, G. D., Walker, J. B., Nesheim, M. E., & Giles, A. R. (2000). Proteolytic processing of human coagulation factor IX by plasmin. Blood, The Journal of the American Society of Hematology, 95(3), 943-951.
79. Saritas, T., Kuppe, C., & Moeller, M. J. (2015). Progress and controversies in unraveling the glomerular filtration mechanism. Current opinion in nephrology and hypertension, 24(3), 208-216.
80. Schroeder Jr, H. W., & Cavacini, L. (2010). Structure and function of immunoglobulins. Journal of allergy and clinical immunology, 125(2), S41-S52
81. Schulte, S. (2009). Half-life extension through albumin fusion technologies. Thrombosis research, 124, S6-S8.
82. Sheffield, W. P., Mamdani, A., Hortelano, G., Gataiance, S., Eltringham-Smith, L., Begbie, M. E., ... & Ofosu, F. A. (2004). Effects of genetic fusion of factor IX to albumin on in vivo clearance in mice and rabbits. British journal of haematology, 126(4), 565-573.
83. Sheffield, W. P., Smith, I. J., Syed, S., & Bhakta, V. (2001). Prolonged in vivo anticoagulant activity of a hirudin–albumin fusion protein secreted from Pichia pastoris. Blood coagulation & fibrinolysis, 12(6), 433-443
84. Sheffield, W. P., McCurdy, T. R., & Bhakta, V. (2005). Fusion to albumin as a means to slow the clearance of small therapeutic proteins using the Pichia pastoris expression system. In Therapeutic Proteins (pp. 145-154). Humana Press

85. Sheffield, W. P., Eltringham-Smith, L. J., Gataiance, S., & Bhakta, V. (2009). A long-lasting, plasmin-activatable thrombin inhibitor aids clot lysis in vitro and does not promote bleeding in vivo. Thrombosis and haemostasis, 101(05), 867-877
86. Sheffield, W. P., & Eltringham-Smith, L. J. (2011). Incorporation of albumin fusion proteins into fibrin clots in vitro and in vivo: comparison of different fusion motifs recognized by factor XIIIa. BMC biotechnology, 11(1), 1-14
87. Sheffield, W. P., Eltringham-Smith, L. J., & Bhakta, V. (2018). Fusion to human serum albumin extends the circulatory half-life and duration of antithrombotic action of the Kunitz protease inhibitor domain of protease nexin 2. Cellular Physiology and Biochemistry, 45(2), 772-782
88. Sleep, D., Cameron, J., & Evans, L. R. (2013). Albumin as a versatile platform for drug half-life extension. Biochimica et Biophysica Acta (BBA)-General Subjects, 1830(12), 5526-5534.
89. Smales, C. M., & James, D. C. (2008). Therapeutic proteins: methods and protocols (Vol. 308). Springer Science & Business Media
90. Strickland, D. K., Au, D. T., Cunfer, P., & Muratoglu, S. C. (2014). Low-density lipoprotein receptor–related protein-1: role in the regulation of vascular integrity. Arteriosclerosis, thrombosis, and vascular biology, 34(3), 487-498
91. Strohl, W. R. (2015). Fusion proteins for half-life extension of biologics as a strategy to make biobetters. BioDrugs, 29(4), 215-239
92. Syed, S., Schuyler, P. D., Kulczycky, M., & Sheffield, W. P. (1997). Potent antithrombin activity and delayed clearance from the circulation characterize recombinant hirudin genetically fused to albumin. Blood, The Journal of the American Society of Hematology, 89(9), 3243-3252
93. Tiede, A. (2015). Half-life extended factor VIII for the treatment of hemophilia A. Journal of Thrombosis and Haemostasis, 13, S176-S179
94. Toutain, P. L., & Bousquet-mélou, A. (2004). Plasma terminal half-life. Journal of veterinary pharmacology and therapeutics, 27(6), 427-439
95. Tully, M., Dimde, M., Weise, C., Pouyan, P., Licha, K., Schirner, M., & Haag, R. (2021). Polyglycerol for half-life extension of proteins—alternative to PEGylation? Biomacromolecules, 22(4), 1406-1416.
96. Ueda, K., Shimizu, M., Ohashi, A., Murata, D., Suzuki, T., Kobayashi, N., ... & Sato, A. (2020). Albumin fusion at the N-terminus or C-terminus of human lactoferrin leads to improved pharmacokinetics and anti-proliferative effects on cancer cell lines. European Journal of Pharmaceutical Sciences, 155, 105551.
97. van Rosmalen, M., Krom, M., & Merkx, M. (2017). Tuning the flexibility of glycine-serine linkers to allow rational design of multidomain proteins. Biochemistry, 56(50), 6565-6574.
98. Vasekar, M., & Craig, T. J. (2012). ACE inhibitor–induced angioedema. Current allergy and asthma reports, 12, 72-78
99. Warshawsky, I., Broze Jr, G. J., & Schwartz, A. L. (1994). The low density lipoprotein receptor-related protein mediates the cellular degradation of tissue factor pathway inhibitor. Proceedings of the National Academy of Sciences, 91(14), 6664-6668.
100. Wood, J. P., Ellery, P. E., Maroney, S. A., & Mast, A. E. (2014). Biology of tissue factor pathway inhibitor. Blood, The Journal of the American Society of Hematology, 123(19), 2934-2943.

101. Wu, Y. (2015). Contact pathway of coagulation and inflammation. Thrombosis journal, 13(1), 1-9
102. Xia, S. W., Wang, Z. M., Sun, S. M., Su, Y., Li, Z. H., Shao, J. J., ... & Zheng, S. Z. (2020). Endoplasmic reticulum stress and protein degradation in chronic liver disease. Pharmacological Research, 161, 105218
103. Yao, L., Xue, X., Yu, P., Ni, Y., & Chen, F. (2018). Evans blue dye: a revisit of its applications in biomedicine. Contrast media & molecular imaging, 2018
104. Yousef, G. M., & Diamandis, E. P. (2001). The new human tissue kallikrein gene family: structure, function, and association to disease. Endocrine reviews, 22(2), 184-204.
105. Zuraw, B. L. (2018). Hereditary angioedema with normal C1 inhibitor: four types and counting. Journal of Allergy and Clinical Immunology, 141(3), 884-885.
106. Zuraw, B., Yasothan, U., & Kirkpatrick, P. (2010). Ecallantide. Nature Reviews Drug Discovery, 9(3)